A
Dissertation
On

A Unified Electrically Simulatable, Electromagnetic Model of TEM cell with DUT for Predicting DUT Radiated Emission

Submitted in Partial fulfillment of the requirement
for the award of Degree of

MASTER OF ENGINEERING
(Electronics & Communication Engineering)

Submitted By:

SRINIVAS DHULIPALLA
College Roll No: 16/E&C/09
University Roll No: 8522

Under the Guidance of:

Dr. ASOK BHATTACHARYYA
(PROFESSOR)
Dept. of Electronics & Communication
Delhi College of Engineering, Delhi.

DEPARTMENT OF ELECTRONICS & COMMUNICATION ENGINEERING
DELHI COLLEGE OF ENGINEERING
DELHI UNIVERSITY

2009-2011

CERTIFICATE

Certified that the thesis work entitled "**A Unified Electrically Simulatable, Electromagnetic Model of TEM cell with DUT for Predicting DUT Radiated Emission**" is bonafied work carried by **SRINIVAS DHULIPALLA** (University Roll No:8522) in partial fulfillment for the award of degree of Master of Engineering in Electronics and Communication Engineering to the University of Delhi during the year 2009-2011. The project report has been approved as it satisfied the academic requirements in respect of thesis work prescribed for the Master of Engineering Degree.

Signature of Guide:

Prof. Asok Bhattacharyya
Electronics & Communication Dept.
Delhi College of Engineering, Delhi.
And also Professor in ECE Dept.,
Faculty of Technology,
University of Delhi.

Signature of co-guide:

Mr. Amit Roy
Senior Member Technical Staff
STMicroelectronics,
Greater Noida.

ACKNOWLEDGEMENT

It is a great pleasure to have the opportunity to extend my heartfelt gratitude to everybody who helped me throughout the course of this project.

It is distinct pleasure to express my deep sense of gratitude and indebtedness to my learned supervisor **Prof. Asok Bhattacharyya,** former H.O.D., Department of Electronics & Communication, Delhi College of Engineering, Delhi and **Mr. Amit Roy,** Senior Member Technical Staff, STMicroelectronics, Greater Noida, for their invaluable guidance, encouragement and patient reviews. I am very thankful to **Prof. Rajiv Kapoor,** H.O.D. Department of Electronics & Communication, Delhi College of Engineering, Delhi, who allows me to do project under the Guidance of **Prof. Asok Bhattacharyya** in collaboration with STMicroelectronics. With their continuous inspiration, valuable guidance in carrying out this work under their effective supervision, encouragement, enlightenment and cooperation, it becomes possible to complete this dissertation and all of them kept on boosting me with time, to put an extra ounce of effort to realize this work.

I would like to sincerely thank Dr. R.N. Biswas for his valuable suggestions to proceed thesis in a bright way.

I would also like to take this opportunity to present my sincere regards to all the faculty members of the Department for their support and encouragement.

I would also like to thanks the management of STMicroelectronics, Greater Noida, for allowing me to use the necessary tools which are required to complete this project work.

I am grateful to my parents for their moral support all the time; they have been always around to cheer me up, in the odd times of this work. I am also thankful to my friends for their unconditional support and motivation during this work.

SRINIVAS DHULIPALLA
M.E. (Electronics & Communication)
College Roll No : 16/E&C/09
University Roll No : 8522
Department of Electronics & Communication Engineering
Delhi College of Engineering, Delhi-110042.

ABSTRACT

Electromagnetic Compliance is now an essential part of the specification. Meeting these complex specifications is now a very challenging task. Most often, EM radiation behaviour can only be estimated in the last stages of back end simulation followed by EM field solution. In this work, we establish a modelling methodology where we first convert the complex geometry of the Transverse Electromagnetic Cell(TEM), which is a standard instrument of EM emission measurement for compliance testing. The complex geometry of the TEM cell is converted to a simple geometry through the Schwartz-Cristoffel transformation, thereby allowing a closed form solution. From this closed form expression, we obtain the electrical equivalent circuit of the TEM cell. We also demonstrate the methodology of converting the SOC's geometry and into an antenna model, which is followed by conversion of the antenna model to an electrical equivalent. Finally, we unify these two models obtained into one electrical model which is used to predict the Radiated Emission captured by the TEM cell measurement. The model and the tool developed from it allow prediction of EM radiation from a SoC at an early stage of design**.** Finally we made an attempt to calculate the characteristic impedance of a GTEM (GIGA HERTZ) cell and computed the electric field, flux lines and magnetic fields of an GTEM cell using FEM(Maxwell 2D).

TABLE OF CONTENTS PAGE NO

LIST OF FIGURES

1. INTRODUCTION

Operation of digital integrated circuits (ICs) drive the electromagnetic emissions of electronics system, hence ICs like microprocessors and microcontrollers can be considered as primary source of electromagnetic emissions (EMEs). Sharp rise/fall of the pulsed current flowing through IC package leads/wirebond excites IC direct radiations of interfering electromagnetic fields. Furthermore steep current and voltages glitches on the IC power supplies which are feeding the input/output(I/O) pad of the IC and the signals carried by the I/O pad results in the noise source which drives the traces of the PCB as an antenna resulting in what is called as Conducted Emission. IC radiated and conducted emissions heavily influence the Electromagnetic Compliance (EMC) features of the electronic apparatus, hence the right selections of the ICs, from the EME point of view, implies a reduced number of EMI filters at the PCB and system level, necessary to compliant with system level EMC requirements .

Almost any electrical transitions with sharp edges, such as clocks, data, address and control, produce electromagnetic radiation. As performance requirements increase, clock speeds have also increased. The transition edge, or in engineering terms, the slew rate, has become faster and faster as the need for meeting set up and hold time has become harder to meet. Set up is the time needed for a data pulse to be stable before the rising edge of the clock, and hold time is the time for the data pulse to remain stable after the edge of the clock

Clocks are no longer fed to only one or two devices on circuit boards. Rather, they are being distributed all over the circuit board. Also, increased memory requirements, and other loads on the clock lines, have significantly contributed to electromagnetic radiation. EMI is linearly proportional to current, the area of the current loop, and with the square of frequency. EMI is defined as $EMI = kIAf^2$ where I is the current, A is the loop area, f is the frequency, and k is the constant depending on PCB materials and other factors. There are two types of EMI radiation: Differential Mode and Common Mode . Current loops formed between traces and the ground plane on PC add-in cards and motherboards cause the Differential Mode. These loops act as antennas and radiate EMI that may exceed FCC limits. Localized ground noise injected into the PC's I/O traces and cable causes Common Mode radiation. Since these cables and traces are long, they act as antennas. For this reason it is now mandatory specifications for the

microcontroller and microprocessor designer to compliant with the specification laid down by the system level companies.

The twin standards SAE J1752/3 [14] and IEC 61967-2 [15] has recognizes the importance of the IC emissions and describes the procedures for evaluating the procedures of Electromagnetic compatibility of the integrated circuits. These procedures call for the IC to be mounted on 10cm X 10cm on the printed circuit board with IC being evaluated on one side and other component need to exercise the IC on the other side of the board. The board is mounted on the opening of the Transverse Electromagnetic Cell (TEM) with the IC facing inside the TEM cell. The TEM cell is an apparatus as shown in Fig.3.1 which involves the use of trapezoidal metallic box with the center septum as the test chamber. The TEM cell is designed which allows the propagation of the transmission-line mode in the region between the box and the septum. To avoid reflections, the cell is designed to have the nominal characteristics impedance of 50 Ω.

In order to interpret the results made in this cell, knowledge of propagating TEM mode is required. This thesis contains a theory of the calculating some basics property of the TEM model of propagation. In this thesis this particular analysis was heavily influenced by [2], [3].[5] Other authors [17], [4], [26] have also tried to do the analysis in their own way. But all the work in [2], [3], [5], [17], [26] was not suitable for the analysis of the complex geometry of today's IC at the early stage of design or was asking for some laboratory measurement to be inserted in their analysis for the prediction of the radiation from the IC.

Studies the EMC of various electronic require accurate measurement techniques to define their EMI characterstics[27].The primary measurement techniques include anechoic chamber , shielded enclosure,Electromagnetic sensors,mode pertubation ,TEM cells etc…In general, an anechoic is a large shielded room. The anechoic chamber provides the uniformity of the EM fields and the shield environment. It is mainly used for the radiated emission and the immunity measurement. In the case of the emission, it is able to generate the real signals, so there is no need to consider the ambient signals. In the case of immunity testing, the anechoic chamber can provide the uniform EM fields, so it will prevent any potential interferences or field distributions. The use of large test areas for measurements and conducting experiments such as an anechoic chamber or open area test site (OATS) are not efficient when the biological samples are very small. For smaller samples a defined area with minimum interference and reflection of the EM

signal area is required and large test chambers do not meet this requirement. On the other hand, a transverse electromagnetic (TEM) cell, which consists of a rectangular coaxial transmission section tapered with coaxial connectors on both ends, is a better choice and provides a uniform EM field in a shielded environment . The usable area of the TEM cell is one-third of volume between the inner and the outer conductors. It is used generally for radiated immunity and emission tests of electronic devices, and biological applications and there are different Numerical techniques to analysize the Differential and integral equations with boundaries involved in calculating EMI/EMC like Separation of variables,Conformal mapping[1] ,Method of moments[23](4Nec2 tool) ,Finite difference method,Finite element method[1](Maxwell 2D), etc.. but we have used conformal mapping to analyise the TEM cell , MoM for modelling DUT, FEM for analysing GTEM cell.

In this work we tried to create one single model suitable for complex geometry of today's IC and presently available measuring instrument and adopted this model for easy computer based simulation. Using this model we can do accurate prediction to certain level even at very early stage of the design.

This thesis is organised into broadly six sections.

In chapter II, we have given the basic fundamental theory required to understand transmission lines and basic knowledge about waveguide , How TE or TM waves develops from TEM wave and TEM waves developed in TEM cell.

In chapter III, we review the existed literature about the TEM cell, the basic properties like electric and magnetic field distribution in a TEM cell, characteristic impedance of a TEM cell, finally higher order modes in a TEM cell.

In chapter IV, we explained detailed modelling of a DUT in different orientations which contributes or doesn't contributes in a TEM cell. the inductance and resistance equivalence of a loop is computed using MoM(4Nec2 tool) , finally analytical expression is formed in a simple way to model DUT.

In chapter V , we explained the flow of a tool and the unified model of a TEM cell loaded with a DUT including simulation results and a few techniques to reduce radiated emission.

In chapter VI , we have given a basic idea about GTEM cell and its characteristic impedance along with the electric and magnetic field using FEM .

2. THEORITICAL BACKGROUND

2.1 Transmission Lines

In this study, understanding of the transmission line theory is required. The TEM cell is fed through a transmission line and one needs to have an understanding of the reflection, transmission of the voltage and current wave on the feed line. A transmission line can be defined in many ways. In general a transmission line is a medium that can be transfer useful energy from one place to another. The transmission line, such as a wire, a coaxial cable, or a waveguide, is used generally as the meaning of the material medium or the structure path for transmitting the energy, such as the EM waves, the cellular phone signals, or the radio signals. However, in this thesis, we would like to use the definition of the transmission line, which is referred from the "Networks and Devices Using Planar Transmission Lines" by Franco Di Paolo, which defines a transmission line as the distributed-parameter network, where voltages and currents can vary in magnitude and phase over their length [28] and analysis of enclosed micro-strip line [28,ch-2].

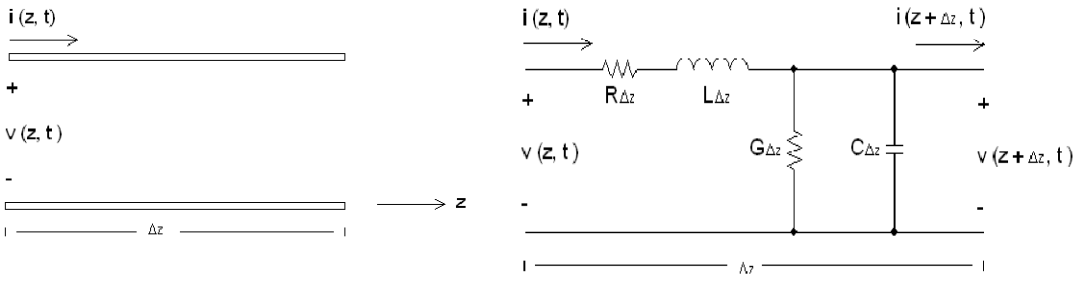

Figure 2.1 The transmission line schematics; (left) voltage and current definition, and (right) lumped element equivalent circuit.

The schematics of a transmission line are shown in Fig. 2.1. The left schematic in Fig. 2.1 shows a two-wire line as two conductors for the TEM wave propagation. This can be drawn as a lumped-element circuit, as shown in the right schematic in Fig 2.1, where R, whose unit is Ohm (Ω)/m, is the series resistance per unit length of both conductors, L, whose unit is Henry (H)/m, is the series inductance per unit length of both conductors. G, whose unit is Siemens (S)/m, is the shunt conductance per unit length, and C, whose unit is Farads (F)/m, is the shunt capacitance per unit length.

2.2 Waveguides:

Since the TEM cell is one kind of waveguides, the theory of the waveguides is also needed to understand the working of the cell. Waveguides are hollow tubes, such as metal tubes, coaxial cables, or strand of glass fibers, used as a conductor or directional transmitter for the electromagnetic waves. They are the EM feed line, and they are commonly used in microwave communications, broadcasting, and radar installations. There are two main types of the waveguide; a rectangular waveguide and a cylindrical waveguide.

The dimensions of the waveguides are related to the wavelength. If the dimensions are very large, the operating frequency will decreased. Therefore, to operate properly, the waveguides need to have a certain minimum diameter relative to the wavelength of the signal. If the waveguide is too narrow or the frequency is too low, which means that the wavelength is too long, the EM fields are not able to propagate. In the waveguide, the EM fields are propagating in various directions. There are two common modes in the waveguide transverse-magnetic (TM) and transverse-electric (TE).

In TM mode, the magnetic lines of flux are perpendicular to the axis of the waveguide. In TE mode, the electric lines of flux are perpendicular to the axis of the waveguide. At the frequencies above the cutoff frequency, which is the lowest frequency at which the waveguide is large enough, the waveguides will function well. Since the TEM cell acts similar to the rectangular waveguide, a brief description of the rectangular waveguide is described here. The rectangular waveguide, which is one of the earliest transmission lines, is used to transport the microwave signal for many past decades, and people still use it today. It is used for many purposes, such as couplers, detectors, isolators, attenuators, and slotted lines. The operating frequencies of the rectangular waveguide are from 1 GHz to over 220 GHz. The rectangular waveguide can be used for high-power systems, millimeter wave systems, and in some precision test applications.

The rectangular waveguide is able to propagate TE and TM modes, but not TEM modes as the TEM cell, since only one conductor is present. The geometry of the rectangular waveguide is shown in Fig. 2.2. We assume that the waveguide is filled with a material of permittivity (ε) and permeability (μ). It is standard convention to have the longest side of the waveguide along the x-axis, so that a is greater than b, where a is the inside width, and b is the inside height.

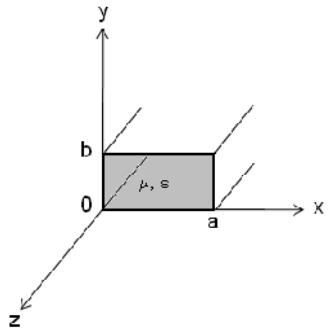

Figure 2.2 : Rectangular Wave Guide

The velocity of propagation for a TEM wave (plane wave or transmission line wave) is referred to as the *phase velocity* (the velocity at which a point of constant phase moves). The phase velocity of a TEM wave is equal to the velocity of energy transport. The phase velocity of a TEM wave travelling in a lossless medium characterized by (μ, ε) is given by

$$u_p = \frac{\omega}{\beta} = \frac{1}{\sqrt{\mu\varepsilon}} \qquad \text{(TEM phase velocity)}$$

The phase velocity of TE or TM mode in a waveguide is defined in the same manner as that of a TEM wave (the velocity at which a point of constant phase moves). We will find, however, that the waveguide phase velocity is not equal to the velocity of energy transport along the waveguide. The velocity at which energy is transported down the length of the waveguide is defined as the *group velocity*.

The differences between the waveguide phase velocity and group velocity can be illustrated using the field equations of the TE or TM rectangular waveguide modes. It can be shown that the field components of general TE and TM waveguide modes can be written as sums and differences of TEM waves. Consider the equation for the *y*-component of the TE mode electric field in a rectangular waveguide.

$$\tilde{E}_y^{TE_{10}} = -\frac{j\omega\mu a}{\pi} H_0 sin\frac{\pi x}{a} e^{-j\beta_{10}z}$$

By applying the trigonometric identity:

$$sin\frac{\pi x}{a} = \frac{1}{2j}\left[e^{j\frac{\pi x}{a}} - e^{-j\frac{\pi x}{a}}\right]$$

this component of the waveguide electric field can be written as

$$\tilde{E}_y^{TE_{10}} = \frac{\omega\mu a}{\pi} H\left[e^{-j(\beta_{10}z+\pi x/a)} - e^{-j(\beta_{10}z-\pi x/a)}\right]_0$$

$$\beta_{10} = k\sqrt{1-\left(\frac{f_{c_{10}}}{f}\right)^2}$$

The two terms in the TE field equation above represent TEM waves moving in the directions shown below.

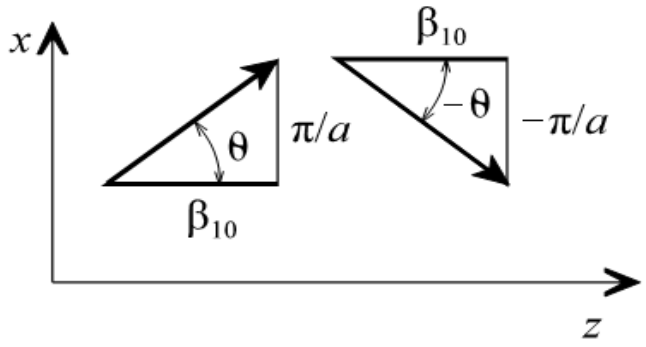

$$\boldsymbol{\theta = tan^{-1}\left(\frac{\pi}{\beta_{10}a}\right)}$$

Figure 2.3: TEM waves directions leads to TE wave

Thus, the TE wave in the rectangular waveguide can be represented as the superposition of two TEM waves reflecting from the upper and lower waveguide walls as they travel down the waveguide.

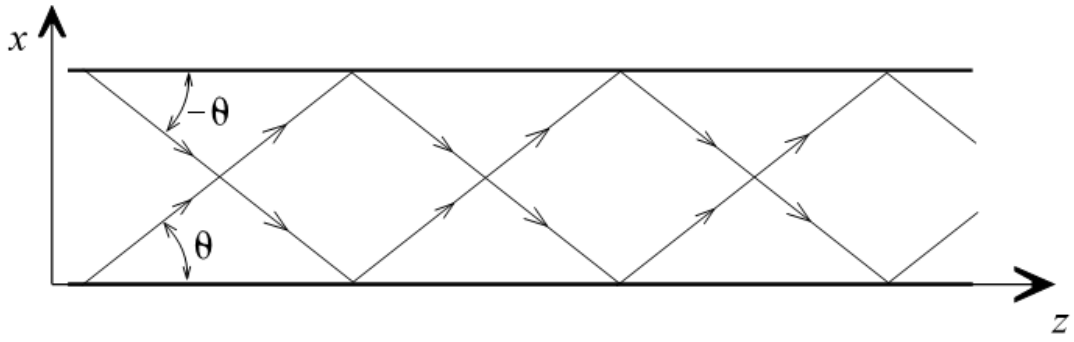

Figure 2.4: TE Waves in the rectangular waveguide can be represented as the superposition of two TEM waves

For the general TE $_{mn}$ of TM $_{mn}$ waves, the phase velocity of the TEM component is given by

$$u_{p_{mn}} = \frac{\omega}{\beta_{mn}}$$

Inserting the equation for the waveguide phase constant β_{mn} gives

$$u_{p_{mn}} = \frac{\omega}{\beta_{mn}} = \frac{\omega}{k\sqrt{1-\left(\frac{f_{c_{mn}}}{f}\right)^2}} = \frac{u_p^{'}}{\sqrt{1-\left(\frac{f_{c_{mn}}}{f}\right)^2}}$$

The waveguide phase velocity represents the speed at which points of constant phase of the component TEM waves travel down the waveguide. The waveguide phase velocity is larger than the TEM wave phase velocity given that the square root in the denominator of the waveguide phase velocity equation is less than unity. The relationship between the waveguide phase velocity, waveguide group velocity, and the TEM component wave velocity is shown below.

$$u_p^{'} = u_{p_{mn}} cos\theta$$

$$cos\theta = \sqrt{1-\left(\frac{f_{c_{mn}}}{f}\right)^2}$$

$$u_{g_{mn}} = u_p^{'}\sqrt{1-\left(\frac{f_{c_{mn}}}{f}\right)^2}$$

$$u_{g_{mn}} u_{p_{mn}} = u_p^{'2}$$

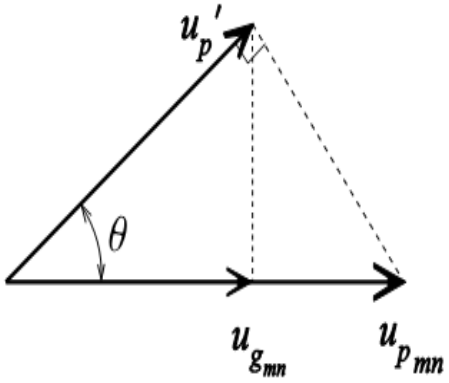

The waveguide group velocity (the velocity of energy transport) is always smaller than the TEM wave phase velocity given the square root term in the numerator of the group velocity equation.

As TEM cell seems to be two rectangular wave guides coupled with an aperture , but in rectangular waveguides TEM waves doesn't propagate ,because of the aperture coupling ,gap is present between septum and outer conductor , due to the gap perturbation TEM waves can propagate in TEM cell ,it was clearly explained in [11] .

3. TRANSVERSE ELECTROMAGNETIC CELL

3.1 TEM Cell:

Transverse electromagnetic (TEM) transmission line cells are devices used to establish standard electromagnetic (EM) fields in a shielded environment. They are triplet transmission lines with the sides closed to prevent radiation of RF energy into the environment and to provide electrical isolation. The cell consists of a section of rectangular coaxial transmission line tapered at each end to adapt to standard coaxial connectors. A uniform TEM field is established inside a cell at any frequency of interest below that for which higher order modes begin to propagate.

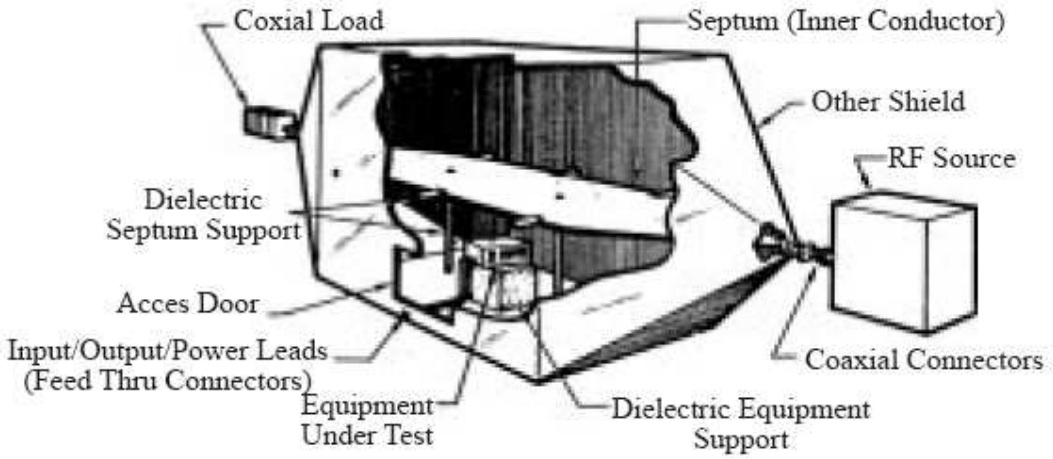

Figure 3.1 : TEM cell

The TEM Cell was designed based on the concept of an expanded planar transmission line operated in a TEM mode to simulate a free space planar wave for susceptibility testing. The TEM cell is mainly a section of a rectangular coaxial transmission line with a flat and wide center conductor and tapered ends acting as transitions to adapt to standard 50Ω coaxial connectors as shown in the figure3.1[26]

In susceptibility tests the power is fed through one input of the TEM cell .From there electromagnetic waves propagate spherically in the tapered part of the cell where in the main volume of the cell the wavefront changes to a planar one. Therefore in the middle part where the DUT (Device under Test) will be situated the field strength is constant along the longitudinal extension unless the presence of a DUT alters the field e.g. with possible conductive or dielectric components. The electromagnetic waves as well as the current in the center conductor are terminated by matched load impedance at the second input of the cell as shown in figure3.2. An advantage over anechoic rooms is the elimination of antennas for establishing the EM fields. In order to reach certain field

strength at the position of the DUT the necessary input power is much lower for a TEM cell than the power of antennas in an anechoic room.

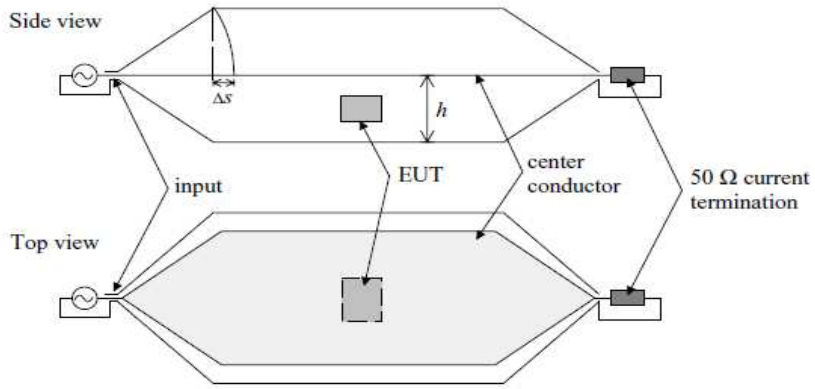

Figure 3.2: Schematic diagram of the TEM cell with the center conductor and the tapered ends. Δs denotes the difference in length of the conductors which limits the usable frequency. The maximum height of the DUT is typically one third of distance h.

To minimize reflections and thus also the standing-wave ratio the cell usually has a characteristic impedance of 50Ω along its length. The size of a DUT is typically restricted to one third of the height h because the EM field is sufficiently uniform only within that region. Furthermore, for larger equipment the effect of the equipment itself on the field strength would be too large as to get reliable results. The well isolated TEM cell neither contributes to nor is affected by any external interference.

As the TEM cell serves as its own transducer it can very well be used for emission tests, again the elimination of antennas is an advantage over OATSs and anechoic rooms. When carrying out emission measurements one or both inputs of the cell are used for monitoring the output power as a result of emissions from the tested equipment. When using both ends one obtains relative phase information which is useful if there is directivity in the emissions. As the emission measurements are performed by monitoring the output Voltage across the input(s) of the cell and not determining the radiated fields directly with the help of antennas, methods have been set up to correlate the data obtained from the TEM cell measurements to the standard OATS measurements as for meaningfully comparison results.

A clear drawback of the TEM cell is the limited useful frequency range due to the cell consisting of three differently shaped parts. Due to the corners of the transitions the length of the inner and outer conductor differs by Δs (see figure3.2). So along the outer

conductor the travel time for a wave is longer by $\Delta t = \frac{\Delta s}{C_0}$. These field distortions give rise to higher mode propagation and thus affect the uniformity of the field inside the cell increasingly at higher frequencies. The highest frequency to use the cell depends mainly on the angle at the transition from the middle part to the tapered ends and thus on the openings angle of the two tapered parts.

The size of the cell is another limiting factor as the cell shows cavity effects like resonances at frequencies at which the dimensions of the cell are about half the wavelength. To increase the Upper frequency limit of the TEM cell with respect to the cavity effects absorbing material can be placed on the walls in order to minimize resonances and reflections. Thereby the useful frequency range can be extended.

The TEM dimensions we have used throughout this thesis are shown in the figure3.3, all the calculations done on the basis of this dimensions. (TEM cell in ST Lab: FCC-TEM-JM1 by Fischer)

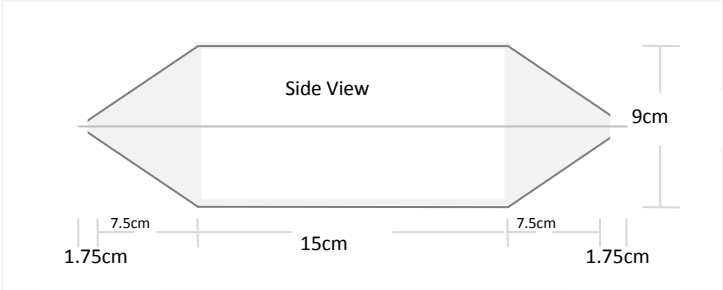

Figure 3.3 : TEM cell Dimensions (TEM cell in ST Lab: FCC-TEM-JM1 by Fischer)

3.2 TEM MODE ANALYSIS*:*

The TEM cell is basically a rectangular coaxial transmission line. In order to understand how an electromagnetic wave can be guided by this structure [2], a brief review of the results from standard transmission line theory is presented. Any multi conductor system, of which the TEM cell is, one, can propagate at least one TEM mode. This mode has many unique properties, not the least of which is that it has no lower cut-off frequency; that is, the TEM mode can propagate through the guide at frequencies all the way down to dc. Another characteristic property of the TEM mode (as its name implies) is that the electric and magnetic field components of this mode lie totally in the transverse plane (i.e., $E_z = H_z = 0$). In the transverse plane, the electric field satisfies Laplace's equation: $\nabla_t^2 \hat{\hat{\varepsilon}} = 0$. This means that the transverse field distribution can be

obtained from the solution of a related static problem. The magnetic field is easily obtained from the electric field as

$$\hat{\bar{H}}^{\pm} = \pm\frac{\overline{a_z} \times \hat{\bar{E}}^{\pm}}{\eta_0} \tag{3.1}$$

Where $\hat{\bar{H}}^{\pm} = \hat{\mathcal{H}}(x,y)e^{j(\omega t \mp yz)}$

$$\hat{\bar{E}}^{\pm} = \hat{\mathcal{E}}(x,y)e^{j(\omega t \mp yz)}$$

$$\eta_0 = \sqrt{\frac{\mu_0}{\varepsilon_0}}$$

Where:

μ_0 is the magnetic permeability

ε_0 is the dielectric permittivity

γ is the propagation constant

$\bar{a}_z$ is a unit vector in the z direction

Many times, it is desirable to characterize TEM waves in terms of the Voltage and current on the line instead of the field quantities, $\bar{E}$ and $\bar{H}$. The Voltage and current are given by the following equations 3.2

$$\hat{V}(z) = \hat{V}_m{}^{+}e^{-\gamma z} + \hat{V}_m{}^{-}e^{-\gamma z} \tag{3.2}$$

$$\hat{I}(z) = \hat{I}_m{}^{+}e^{-\gamma z} + \hat{I}_m{}^{-}e^{-\gamma z} \tag{3.3}$$

Where: $\hat{V}_m{}^{\pm} = -\int_p \hat{\bar{\mathcal{E}}}^{\pm}.\,\bar{dl}$ and

$\hat{I}_m{}^{\pm} = \oint_l \hat{\mathcal{H}}^{\pm}.\,\bar{dl}$

Where p is any path connecting the two conductors in a constant cross-sectional plane and ℓ is a closed path encircling the inner conductor. $\hat{V}_m$and $\hat{I}_m$ are related by a constant which is called the characteristic impedance, Z_O of the line, and is given by equation 3.3

$$Z_0 = \pm\frac{\hat{V}_m{}^{\pm}}{\hat{I}_m{}^{\pm}}. \tag{3.4}$$

If one measures the amplitudes of the forward and backward voltage waves, $\hat{V}_m{}^{\pm}$ then, with a. knowledge of the characteristic impedance, using equ. (3.2) determine the voltage and current anywhere on the line.

The characteristic impedance, Z_O, can also be expressed in terms of the distributed capacitance per unit length of the transmission line, C_O, as follows:

$$Z_0 = \frac{1}{\upsilon C_0} \tag{3.5}$$

Where $\upsilon = \frac{1}{\sqrt{\mu_0 \varepsilon_0}}$ is the phase velocity

Thus knowledge of the distributed capacitance, C_O, completely determines the characteristic impedance. In addition to the characteristic impedance.

3.3 Electric Field Distribution in a TEM cell*:*

The distribution of the electric field of the TEM mode becomes important when one considers source related problems, e.g., the most efficient excitation of the TEM mode will occur when the source current is aligned along the lines of maximum electric field. The electric field distribution as well as the characteristic impedance of the TEM mode can be obtained using the method of conformal transformation to map the cross section of the TEM cell shown in Fig. 3.4 with a symmetrical x-y coordinate system superimposed.

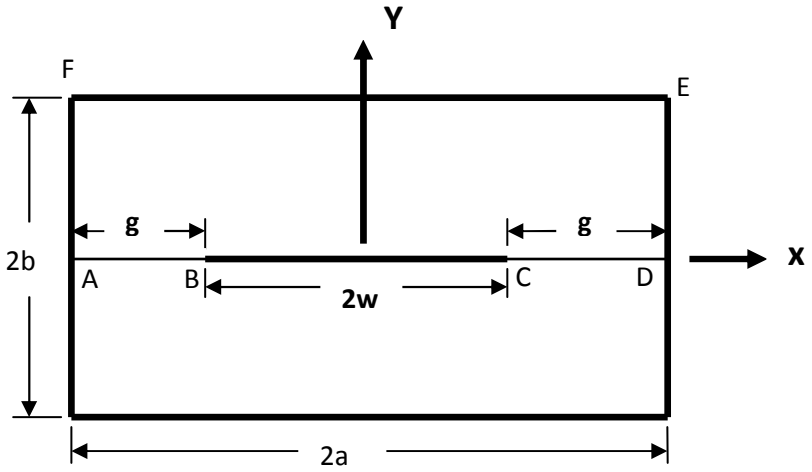

Figure 3.4 Cross section of TEM cell.

into a region for which the solution to Laplace's equation is known. The center septum of width 2w is located symmetrically inside the cell of width 2a and height 2b, and is assumed to have negligible thickness. In addition, the septum is located a distance g from each vertical side wall. For convenience, some key points in the cell have been labelled A through F. The region A-D-E-F may be mapped into the upper half of a complex t-plane via the Schwarz-Christoffel transformation [1] which, due to symmetry, can be expressed in terms of Jacobian elliptic functions [31, pp. 7-15 and 1,ch-9]. The

transformation is given by

$$mz = \int_0^t \frac{dt'}{\left[\left(1-t'^2\right)\left(1-k^2t'^2\right)\right]} \tag{3.6}$$

or alternatively by $t = sn(mz, k)$

where sn is a Jacobian elliptic function of modulus, k,

$$m = \frac{K(k')}{b}$$

And Z=x+iy

with x and y indicating the location of the field point as measured from the center of the TEM cell in the transverse plane. Here K(k) and K(k') are complete elliptic integrals of the first kind of moduli k and k', respectively [1], and

$$k' = [1-k^2]^{1/2} \tag{3.7}$$

The modulus k can be determined from the requirement that

$$\frac{K(k)}{K(k')} = \frac{a}{b}$$

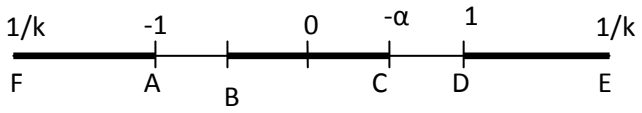

Figure 3.5. Complex t-plane

Under the transformation given by (3.6), the region, A-D-E-F, in the z-plane is mapped into the upper half of the t-plane as shown in Fig. 3.5. Using (3.6), a in Fig.3.5 can be calculated

as $\alpha = sn(mw, k).$ (3.8)

For convenience, we now make an intermediate transformation from the t-plane to a complex u-plane defined by

$$u = t/\alpha \tag{3.9}$$

The u-plane is shown in Fig.3.6.

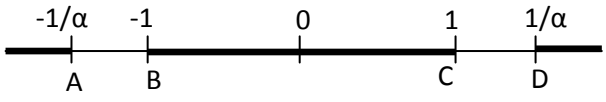

Figure 3.6. Complex u-plane.

Finally, we map the upper-half of the u-plane into a complex Z-plane defined by

$$u = sn(\chi, \alpha) \tag{3.10}$$

The Z-plane is shown in Fig.3.7 and α' is defined analogously to k'. In order to calculate the electric field, we must find the complex potential, F, which is given by

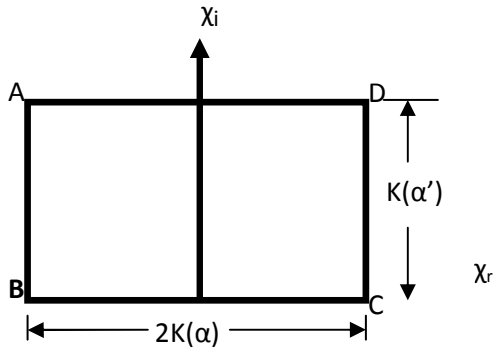

Figure 3.7. Complex χ-plane.

$$F = \phi(\chi) + i\psi(\chi) \tag{3.11}$$

Where

$\phi(\chi)$ is the potential function

ψ(χ) is the stream function

F satisfies the Cauchy-Riemann equations.

In addition, the potential, $\phi(\chi)$,must satisfy the following boundary conditions

$\phi(\chi)$ =0 on BC and

$\phi(\chi)$ =V on AD.

It is easily verified that the following solution satisfies all of the above requirements

$$\phi(\chi) = \frac{V_{\chi_i}}{K(\alpha')} \tag{3.12}$$

$$\psi(\chi) = \frac{V_{\chi_r}}{K(\alpha')} \tag{3.13}$$

Where $\chi = \chi_r + i\chi_i$.

The electric field, E, is defined by

$$E = \hat{\mathcal{E}}_x + i\hat{\mathcal{E}}_y = -\left(\frac{\partial}{\partial x}\phi + i\frac{\partial}{\partial x}\right)^{\phi}$$

$$= -\left(\frac{\partial}{\partial x}\phi + i\frac{\partial \psi}{\partial x}\right) = -\frac{d}{dx}F^* \tag{3.14}$$

The real part of E gives the x component of the electric field, and the imaginary part of E gives the y component of the electric field. dF/dz may be calculated as follows:

$$\frac{dF}{dx} = \frac{dF}{d\chi}\frac{d\chi}{du}\frac{du}{dt}\frac{dt}{dz} \tag{3.15}$$

Using (3.7).(3.8) and (3.10) through (3.15), dF/dz may be evaluated as

$$\frac{dF}{d\chi} = \frac{iVm}{K(\alpha')} \tag{3.16}$$

$$\frac{du}{d\chi} = cn(\chi).dn(\chi) \tag{3.17}$$

$$\frac{du}{dt} = \frac{1}{\alpha} \tag{3.18}$$

$$\frac{dt}{dz} = cn(mz).dn(mz) \tag{3.19}$$

by substituting the above equations

$$\frac{dF}{dx} = \frac{iVm}{K(\alpha')}.\frac{1}{cn(\chi).dn(\chi)}.\frac{1}{\alpha}.cn(mz)dn(mz) \tag{3.20}$$

$$t = \alpha.sn(\chi,\alpha) \tag{3.21}$$

From the elliptic integral properties

$$sn(mz,k) = \frac{sn(\chi,\alpha)}{sn(mw,\alpha)} \tag{3.22}$$

$$dn(\chi,\mathrm{k}) = \sqrt{1-\alpha^2\mathrm{sn}^2(\chi,\alpha)} \tag{3.23}$$

$$cn(\chi,\mathrm{k}) = \sqrt{1-\mathrm{sn}^2(\chi,\alpha)} \tag{3.24}$$

by substituting the equations (3.22),(3.23) and (3.24) in (3.20)

$$\frac{dF}{dz} = \frac{iVm}{K(\alpha')}.\frac{dn(mz)}{\sqrt{1-\frac{\mathrm{sn}^2(\mathrm{mz},\mathrm{k})}{\mathrm{sn}^2(\mathrm{mw},\mathrm{k})}}.\mathrm{sn}(\mathrm{mw},\mathrm{k})} \tag{3.25}$$

$$\frac{dF}{dz} = \frac{-iVmdn(mz)}{K(\alpha')[P_0(z)]^{1/2}} \tag{3.26}$$

Where $P_O(z) = [sn^2(mw) - sn^2(mz)]$

and dn is another Jacobian elliptic function all of which have mod k. Thus the magnitude squared of the electric field, E_o^2, is given by

$$E_o^2 = \left[\frac{V_m}{K(\alpha')}\right]^2 \left|\frac{dn^2(mz)}{sn^2(mw)-sn^2(mz)}\right| \tag{3.27}$$

It is easy to see from (3.27) that for z = +w, E_o^2 goes to infinity as expected from the edge condition. Equation (3.27) was evaluated numerically for a typical TEM cell geometry shown in figure 3.3 and used to calculate the x and y components of the electric field, as well as the magnitude and polarization angle of the electric field defined by

$$\theta = arctan\left(\frac{E_y}{E_x}\right) \tag{3.28}$$

The modulus k for the dimensions shown in figure 3.3 is 0.99977≈1 then the electric field E has been reduced by applying sn(mz)=tanh(mz) , cn(mz)=sech(mz) , dn(mz)=sqrt(1-$k^2$$sn^2$(mz)), in final transformation the modulus α has also been computed as 0.99987≈1 then $K(\alpha') = {}^{\pi}/_{2}$ then the electric field E can be computed by applying one volt to the empty TEM cell, the electric field magnitude is plotted in Fig.3.8

$$E = \sqrt{\left[\frac{1}{\pi/2}\right]^2 \left|\frac{\sqrt{1-k^2tanh^2(mz)}}{tanh^2(mw)-tanh^2(mz)}\right|} \tag{3.29}$$

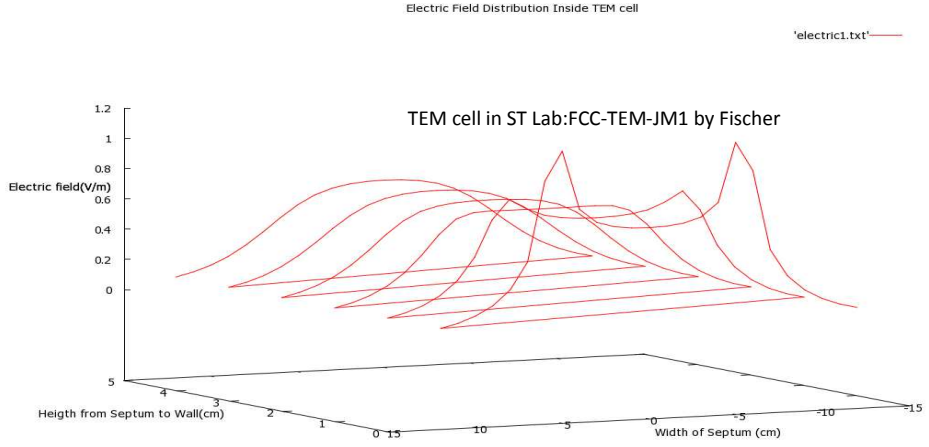

Figure 3.8: Electric Field distribution of an empty TEM cell

Since it is well known that capacitance is invariant under a conformal-transformation, we may use the geometry of Fig 3.7. to also calculate the capacitance of the TEM cell. From that figure 3.7, it is evident that the capacitance is just given by the ordinary parallel plate capacitor formula, that is

$$\frac{C}{\varepsilon_0} = 2\frac{K(\alpha)}{K(\alpha')} \tag{3.30}$$

Therefore, the total capacitance, C_O, of the TEM cell transmission line per unit length is just twice that given by

$$\frac{C}{\varepsilon_0} = 4\frac{K(\alpha)}{K(\alpha')}. \tag{3.31}$$

3.4 Magnetic Field Distribution of the TEM cell*:*

For either the forward or reflected wave the magnetic field is given by the TEM requirement from the electric field. If the electric field is normalized with V/b ,then actual electric field is $\vec{E}(x,y).V/b$, and the magnetic field without reflections is

$$\vec{H}(x,y) = \pm\overleftrightarrow{Y}.\vec{E}(x,y).V/b \tag{3.32}$$

The expression with reflections is

$$\vec{H}(x,y) = \pm\overleftrightarrow{Y}.\vec{E}(x,y).Z_0I/b \tag{3.33}$$

where $\overleftrightarrow{Y}$ is the dyadic wave admittance

$\overleftrightarrow{Y} = Y(\hat{\jmath}\hat{\imath} - \hat{\imath}\hat{\jmath})$ and $Y = \sqrt{\frac{\varepsilon_0}{\mu_0}} = \frac{1}{377\Omega}$

the above expression illustrates that without reflections the magnetic field is transverse to the electric field and has the magnitude given by the electric field magnitude divided by the impedance of free space .

3.5 Characteristic Impedance*:*

Characteristic Impedance is derived that exhibits the dimensions of the TEM cell explicitly, thus facilitating the design of a cell with given characteristic impedance. The approximate form is derived in appendix-1 [32]and is given by

$$\frac{C}{\varepsilon_0} = 4\left[\frac{w}{b} + \frac{2}{\pi}ln\left(1 + coth\frac{\pi g}{2b}\right)\right] \tag{3.34}$$

where g, b, and w are defined in Fig.3.3. Equation (3.34) is a good approximation of the more complicated but exact expression under the following conditions:$\frac{a}{b} \geq 1$ and $\frac{w}{b} \geq \frac{1}{2}$

Using (3.5) and (3.31), the characteristic impedance of the TEM cell is found to be

$$Z_o = \frac{\eta_0}{4}\frac{K(\alpha')}{K(\alpha)} \tag{3.35}$$

and the approximate form using (3.34) is then

$$Z_o = \frac{\eta_0}{4\left[\frac{w}{b} + \frac{2}{\pi} ln\left(1 + coth\frac{\pi g}{2b}\right)\right]} \tag{3.36}$$

Using the above equation we can calculate the characteristic Impedance of a TEM cell Assuming the TEM cell as pure transmission line ,replacing with the inductance and capacitance. i.e calculated from $Z_o = \sqrt{\frac{L}{C}}$ capacitance is calculated using equ(3.34) Substituting the Z_o and C we can get L.

3.6 Mode Excitation:

When the electric or magnetic current source, such as a monopole antenna, is inserted in the waveguide, we need to consider the electric current source ($\bar{J}$), whose location is between two transverse planes at z_1 and z_2, as shown in Fig. 3.5. The $E^{\pm}$, and $H^{\pm}$+ fields are then generated. As we can see in Fig. 3.5, the E^{+} , and H^{+}+ fields are travelling in the +z direction, and the E^{-} , and H^{-} fields are travelling in the –z direction. The E and H fields [5] can be formulated in terms of the waveguide modes as given below

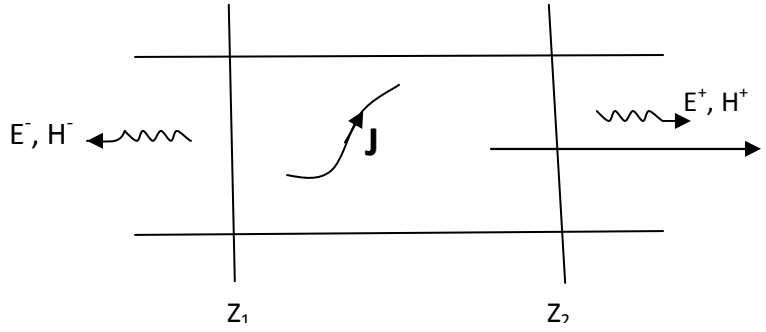

Figure 3.9: E and H fields when a electric current source located in between transverse planes z_1 and z_2 .

$E^{+} = \sum_n C_n^{+}(e_n + e_{zn})e^{-j\beta_n z}$ $z > z_2$

$H^{+} = \sum_n C_n^{+}(h_n + h_{zn})e^{-j\beta_n z}$ $z > z_2$

$E^{-} = \sum_n C_n^{-}(e_n - e_{zn})e^{j\beta_n z}$ $z < z_1$

$H^{-} = \sum_n C_n^{-}(h_n - h_{zn})e^{j\beta_n z}$ $z < z_1$

In above equations n is a general summation index and implies a summation over all possible TE and TM modes .The unknown amplitudes C_n may be determined by

an application of the Lorentz reciprocity formula . For the volume V ,choose that bounded by the waveguide walls and cross-sectional planes located at z_1 and z_2 in figure. Let the field E_1, H1 to be used in the Lorentz reciprocity formula, be the field radiated by the current source .This field is given by above equations. For the field E_2 ,H_2 ,choose the nth waveguide mode E_n^- ,H_n^-; that is,

$$E_2 = E_n^- = (e_n + e_{zn})e^{j\beta_n z}$$

$$H_2 = H_n^- = (-h_n + h_{zn})e^{j\beta_n z}$$

From Lorentz reciprocity formula [10]

$$\oint_S (E_1 \times H_n^- - E_n^- \times H_1) \cdot n dS = \int_V E_n^- \cdot J dV \tag{3.37}$$

Since the field E_2 ,H_2 is a source –free solution (J_2=0) within V. The surface integral is zero over the waveguide walls by virtue of the boundary condition $n \times E_1 = n \times E_n^- = 0$. since this modes are orthogonal ,i.e.,

$$\int_{S_0} E_m^{\pm} \times H_n^{\pm} \cdot n dS = 0 \quad n \neq m \tag{3.38}$$

All the terms except the nth in the expansion of E_1,H_1 vanish when integrated over the waveguide cross section S_0. Thus we have

$$\int_{Z_2} C_n^+[(e_n + e_{zn}) \times (-h_n + h_{zn}) - (e_n - e_{zn}) \times (h_n + h_{zn})].a_z dS - \int_{Z_1} C_n^-[(e_n - e_{zn}) \times (-h_n + h_{zn}) - (e_n - e_{zn}) \times (-h_n + h_{zn})].a_z dS = -2C_n^+ \int_{z_2} e_n \times h_n \cdot a_z dS = \int_V E_n^- \cdot J dV \tag{3.39}$$

Since the integral over the cross section at z_1 vanishes identically. Hence C_n^+ is given by

$$C_n^+ = -\frac{1}{P_n}\int_V E_n^- \cdot J dV = -\frac{1}{P_n}\int_V (e_n - e_{zn}) \cdot J e^{j\beta_n z} dV \tag{3.40}$$

If E_n^+,H_n^+ is chosen for the field E_2 ,H_2 we obtain

$$C_n^+ = -\frac{1}{P_n}\int_V E_n^+ \cdot J dV = -\frac{1}{P_n}\int_V (e_n + e_{zn}) \cdot J e^{-j\beta_n z} dV \tag{3.41}$$

Where

$$P_n = 2\int_{S_0} e_n \times h_n \cdot a_z dS$$

And S_0 is a cross-sectional surface of the waveguide . the normalization constant P_n depends on the choice of expressions used for e_n and h_n , the later being arbitrary.

$$P_e = \frac{|A^+|^2 V^2}{2\, Z_0} \tag{3.42}$$

where A^+ Is the excitation factor

$$A^+ = -\frac{Z_0}{2V^2}\int_\tau E_n^- \cdot J dv' \tag{3.42.1}$$

V is the voltage between the inner and outer conductors

Z_0 is the Characteristic impedance

τ is the volume enclosing all sources

$E^{(-)}$ is the electric field of the negative –z propagating wave

J is the source current density

considering an electric dipole , the volume integral in above equation (3.42.1)reduces to

$$\int_\tau J.E_n^- dv' = E_0(x_0, y_0, z_0) I l_{eff} cos\hat{\theta} \tag{3.43}$$

where

(x_0, y_0, z_0) is the source point

$\hat{\theta}$ is the angle between the dipole and the electric field at the source point

l_{eff} is the effective dipole length

E_0 is the magnitude of the electric field at the source point

I is the magnitude of the dipole current

Using (3.42) , (3.43) and (3.44)

The power carried by the TEM mode of a transmission line that is exited by an elementary electric dipole is given by

$$P_e = \frac{Z_0}{2}\left(l_{eff}\frac{E_0 I cos\hat{\theta}}{2V}\right)^2 \tag{3.44}$$

$\hat{\theta}$ places a major role in DUT orientation i.e if the dipole is placed horizontal to the septum then the angle made by the dipole with electric field emitting from the septum is 90^0 , then $cos\hat{\theta}$ is 0 which means the power carried by the TEM mode of a transmission line is zero. In the same way it carries maximum power when the dipole is perpendicular to septum i.e then $\hat{\theta}$=0^0

If instead of an electric dipole , source were a magnetic dipole , then the radiated power is given by

$$P_m = \frac{Z_0}{2}\left(\frac{2\pi A}{\lambda_0}\frac{E_0 I_m cos\hat{\phi}}{2V}\right)^2 \quad (3.45)$$

where

λ_0 is the wavelength

$A = \pi r^2$ is the area of the loop representing the magnetic dipole

I_m is the equivalent magnetic current

$\hat{\phi}$ is the angle between the loop normal and the magnetic field at the source point.

When analysing magnetic loops $\hat{\phi}$ places a role in DUT orientation i.e if the magnetic loop is placed horizontal to the septum , the normal to the loop makes an angle 90^0 with the magnetic field produced by the septum . Then the power carried by the TEM wave is zero. moving towards magnetic loop placed vertically , there are again two cases i.e normal of the loop makes 90^0 with the magnetic field and normal of the loop can make 0^0 with the magnetic field produced by the septum (is clearly explained in DUT orientation).

3.7 Higher order modes*:*

Ideally a transmission line should subject equipment under test to an electric field waveform similar to that it would have experienced in free space illumination. This means that the pulse incident on the equipment under test should be a pure TEM wave with a near planar or spherical wavefront, as in free space propagation. However, multiple scattering of the transmission line structure and equipment under test, and reflections from the termination, produce features in the resulting waveform which are markedly different from the free-space case

Transmission lines with open waveguide like structure do not possess a denumerable infinite set of discrete modes as do closed waveguides. In general, the normal modes consist of a finite set of bound modes together with a continuous modal spectrum bounded at infinity. When line is operated at low frequencies, the leaky mode component is not present and the field consists only of the bound and residual waves. So the TEM mode is predominant in this case. As the frequency is increased, leaky wave modes contained within the non-physical spectral gap region are able to make their

presence felt indirectly by influencing a now much stronger residual wave. At higher frequencies still, the leaky waves become physical, directly influencing the behavior of the line no longer operates as a TEM mode transmission line . However TEM mode propagates at all frequencies.

With increasing frequency, higher order modes (HOM) can propagate above their cutoff frequency[24]. These cutoff frequencies depend on the cross-sectional geometry of the transmission line. In the case of a TEM cell, both the dimensions of the outer conductor and the location and dimensions of the equipment under test determine HOM propagation. As the cross-sectional geometry changes along the direction of propagation, the cutoff frequencies of HOM also changes. This behavior can be termed local cutoff frequency .

3.7.1 Propagation Modes

The fundamental of all modes is the TEM mode which propagates from zero frequency, but at higher frequencies higher order TE (or H-modes) and TM (or E-modes) modes starts appearing. In TE mode $E_z = 0; H_z \neq 0$ and in TM mode $H_z = 0; E_z \neq 0$. The lowest order members of these two families are the TE_{01} and TM_{01} modes which is first to appear depends on the aspect ratio of the cross-section. For a > b it will be the TE_{01} and for the converse, the TM_{01}; when a = b, both appear together as a degenerate pair of modes . The transverse inhomogeneity of the transmission line causes coupling between the TE and TM modes such that neither can exist separately. The resultant hybrid models need at least two scalar variables for their representation.

3.7.2 Higher Order Modes

Higher order modes are excited by changes of the cross section or by the finite conductivity of realistic transmission line conductor. The amplitude of a higher order modes depends on the excitation as well as on the capability for propagation. Modes which are excited by the TEM modes and inevitable for geometrical reasons are called essential modes. Others, excited by disturbances in the geometry or little discontinuities and reaching only small amplitudes are called non- essential modes .

TEM (Transverse Electro Magnetic) waves are characterized by the fact that both the electric vector(E-field) and the magnetic vector(H-Field) are perpendicular to each other and to the direction of propagation. A TEM cell will not only propagate a single TEM mode at all frequencies, but also a set of Transverse Electric and Transverse

Magnetic higher order modes TE_{mn} and TM_{mn} at frequencies above their respective cut-off frequencies $f_{c(mn)}$. The TEM mode propagates through the tapered ends of the cell without significant alteration. Each higher-order mode, however, is always reflected at some point within the taper where it becomes too small to propagate the mode. This is the point where the cross-section of the taper has narrowed to that of a waveguide whose cut-off frequency is lower than the field frequency. The propagating energy in the higher-order mode undergoes multiple reflections, end to end, with in the cell, until it is dissipated.

With TEM cell, higher order modes cannot propagate in the tapered region of the cell. This means that higher order modes can exist only in the working volume range of transmission line. The higher order modes appear in TEM cell at sharply defined frequencies. These sharp cutoff frequencies excite one or more resonant frequencies which ultimately destroys the uniform field distribution inside the cells. As the size of TEM cell is increased to accommodate higher frequency and huge size of equipment under test the higher order modes starts to appear at low frequencies compared to the frequency range of usage.

Working out the forms of the higher order mode in open structure like ours is nontrivial task. To obtain the proper boundary condition we discretised the field expression that satisfies Helmholtz equation rather than Laplace's equation and take more number of higher order modes into account. By doing this we can properly characterize the wave behavior of the field near the edge with higher order accuracy and stable results. Also any spatial derivative of the longitudinal field becomes infinite as a sharp edge is approached; the accuracy of the field solution near the edge is very sensitive to any sources of error .

The 2-D equation governing the transmission line, to study higher order modes, is Helmholtz equation

$$(\nabla^2 + k^2)V(x, y) = 0 \tag{3.46}$$

with Dirichlet boundary condition (i.e. fixed boundary values) for transverse electric field component given by Eq. 3.2 and Eq. 3.3,

$$V(x, b) = V_0 \ ; \qquad -a \leq x \leq a \tag{3.47}$$

$$V(x, 0) = 0; \qquad -\infty \leq x \leq \infty \tag{3.48}$$

and with Neumann boundary condition for longitudinal magnetic field component given by Eq. 3.49,

$$\frac{\partial V(x,y)}{\partial n} = 0; \tag{3.49}$$

over the cross-section contour. Here $k^2 = \omega^2 \mu_0 \varepsilon_0$ and V = E_z or H_z for TE_{mn} or TM_{mn} modes respectively. E_z and H_z are the longitudinal components of electric and magnetic fields .

The useful frequency range of the TEM cell for electromagnetic interference measurements is limited by the cutoff frequencies of the higher order transverse electric (TE) and transverse magnetic (TM) modes and the appearance of resonances due to reflections at taper sections. The higher order mode resonances appear at sharply defined frequencies. Resonances of higher order modes determine the usable bandwidth of a TEM cell. Thus, there may exist frequency windows between resonances where field variations become predictable and TEM cell usage is still quite valid. The cutoff frequencies may be used to predict the frequencies of higher order TEM cell resonances and measures may be selected to suppress resonances of higher order modes and the bandwidth of the transmission line can be expanded without affecting the transverse electromagnetic (TEM) mode. The cutoff frequencies of the higher order modes of a TEM cell are derived from the eigenvalue k^2 of the governing equation Eq. 3.46

Knowing normalized cutoff frequency of transmission line is important in calculating the resonant length of the transmission line. However, determining them is non-trivial since the tapered section affects each higher order mode differently . The structure and properties of transmission line modes are determined by solving the two dimensional eigenvalue problems formed by Eq. 3.46. To each eigenvalue k^2 and corresponding eigenfunction represents a different mode, the cutoff frequency of which is given by Eq. 3.50.

$$f_c = \frac{k}{2\pi\epsilon\mu} = \frac{ck}{2\pi} \tag{3.50}$$

c is velocity of light in free air.

The variational principle explains the significance of eigenvalue problem concerning waveguide or cavity modes, independent of its explicit or implicit usage. It allows much more accurate determination of field eigenvalue than field distributions with the same amount of numerical efforts, owing to the stationary property of the solutions. In other words, the computed eigenvalue are not sensitive to the errors in the field distributions. On the other hand, even if the eigenvalue are calculated with sufficient accuracy, the field distributions may still be of poor accuracy.

At certain frequencies a resonance condition is satisfied, in which the cell's effective length for the mode is 'p' half guide wavelengths long (p=1, 2, 3…….). at these resonant frequencies $f_{R(mnp)}$ a TE_{mnp} resonant field pattern exists. Thus the TE_{mn} mode in a given TEM cell has one cutoff frequency $f_{c(mn)}$ and an infinite set of resonant frequencies, $f_{R(mnp)}$ with p=1,2,3…..The same is true for the TM_{mn} higher –order modes, although these only occur at higher frequencies. The resonant frequencies $f_{R(mnp)}$ are calculated from the values of $f_{c(mn)}$ and the cell's length and taper dimensions ,

$$f_{R(mnp)}^2 = f_{c(mn)}^2 + \left(\frac{pc}{2L_{mn}}\right)^2 \tag{3.51}$$

$$L_{mn} = L_c + X_{mn}L_E$$

L_c is the length of the uniform –cross-section center part of the cell ,L_E is the length (along the center line) of the two tapered ends, and X_{mn} Is the fraction of the two ends included in the value of L_{mn} ,fraction X_{mn} is empirically determined and is different for each cell as well as each mode .It can change 0.8 for TE_{01} mode to 0.5 for the TE_{10} and TE_{11} modes The TE_{01} mode in a small gap TEM cell has a strong gap-fringing fields, while not exhibiting significant fields in the central test area, Therefore although the TE_{01} causes the first possible resonance , it is usually not exited unless a large test object or some other perturbation is present .

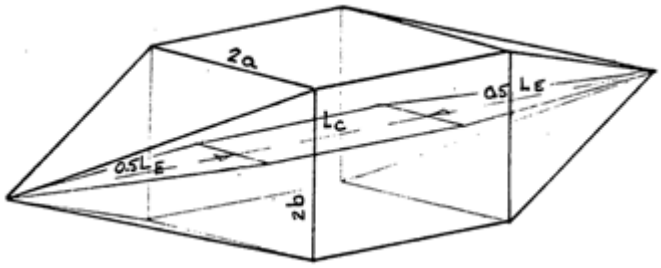

Figure 3.10: The length of the cell is $L=L_c+L_E$

4. DUT MODELLING

4.1 Introduction

IC emissions affect both the internal workings and the total external emissions of the system in which the device is placed. Internal to a system, the near-field emissions from the IC, its package, and its immediately-connected traces can couple to nearby, noise-sensitive circuits, causing degraded system performance or even system malfunction. External to a system, the total emissions receive contributions from the IC emissions via several mechanisms, such as radiation from apertures, which are coupled to the IC via direct or indirect excitation of cavity resonances, and radiation from external connecting cables, which are coupled to the IC via cavity resonances or unintentional PCB conduction paths. As clock frequencies increase and electronic systems proliferate, the impact of package and IC-level EMC on system-level EMC performance will rise.

The time-varying signals on the IC, the chip-to-package bond wires, and the package lead frame are the sources of radiation into the stripline section of the TEM cell. The stripline waveguide supports an infinite number of modes, which can be propagating or evanescent depending on the frequency. At the frequencies of interest, only the dominant TEM mode propagates power, and the coupling from the source to the TEM mode determines how much power exits the TEM cell to the measurement equipment. Since an arbitrary source in this waveguide will excite an infinite number of modes, the signals on the IC and its package are also capable of coupling to higher order modes. The coupling from an arbitrary current source to the TEM cell’s coaxial waveguide modes can be calculated by combining a field-match.

The contributions of various parts of the IC to the total IC emissions can be calculated using the electromagnetic model of the signal path's radiation resistance. First, the geometry of the signal path is identified. Then, the radiation resistance is calculated. A SPICE model of the portion of the IC which is under investigation determines the time-domain currents on the signal paths, and a Fourier transform yields the frequency domain excitation of the TEM cell. As an example, the emissions due to the switching of an output port of a microcontroller is modelled and compared to the overall measured emissions of the chip and its package by Andy Engel from Motorola [4].

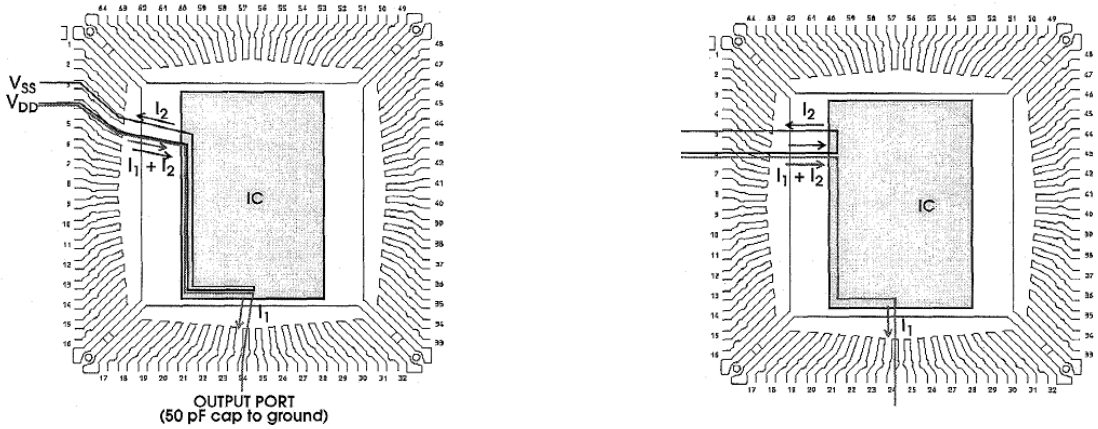

Figure 4.1: Actual (left) and simplified (right) paths for IC currents caused by switching an output port.

The figures 4.1 are viewed from above the package, looking down at the IC and the package lead frame. I_1 is the current on the output pin and I_2 is the shoot-through current. When the output driver switches, two currents are introduced to the IC and its package: the current which is needed to charge or discharge the load capacitance and the shoot-through current which occurs in the short interval when the n- and p-channel device in the driver are simultaneously turned on. The IC and package paths over which the currents travel are shown in figure 4.1.

The electromagnetic model for the radiation resistance uses two separate simplified current paths, also shown in figure 4.1. The output port current I_1 travels on VDD and the output pin when the output changes from low to high and the output port current travels on VSS and the output pin when the output changes from high to low. Since the VDD and VSS pins are adjacent, the path of I_1**,** is simplified by assuming that the physical path is the same for both types of transitions. The path of the shoot-through current I_2 is greatly reduced because the on- chip path of this current consists of two opposing currents which are physically very close together, and the net contribution of the on-chip path to the radiation resistance is negligible. The radiation resistance calculation also takes into account the vertical feeds from the outer shell of the TEM cell. The vertical height was assumed to be the height of the package legs plus the chip height; the effects of the bond wires which connect the lead frame and the chip were taken into account to some extent by connecting the package legs with the shortest possible distance.

In the TEM cell, the package and IC are placed inside the TEM cell using a special PCB (figure 4.2). On the interior side, the IC is centered on the PCB. The rest of

the interior side of the PCB is mostly ground plane so as to preserve the electromagnetic wave guiding properties of the TEM cell. Via holes connect the package leads to the bias and terminating circuitry, which are on the outside of the TEM cell. The view shown in figure 4.1 is parallel to the center conductor and above the outer shell of the TEM cell by the height of the package legs.

Figure 4.2: Placement of a DUT(IC) on PCB for EMC measurement.

The PCB kept on TEM cell using side locks of the TEM cell as shown in the figure 4.3. Facing IC interior to the TEM cell.

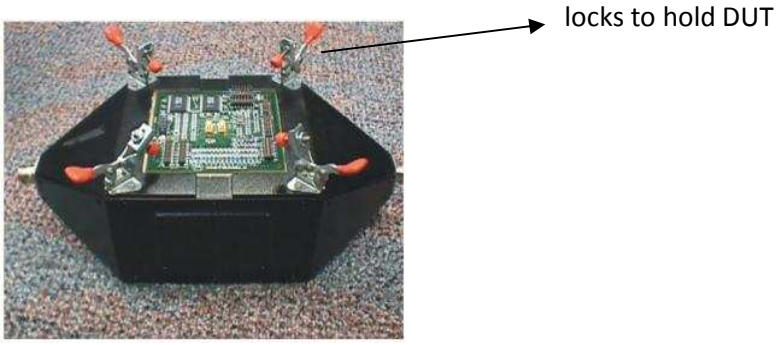

Figure 4.3: Mounting DUT in TEM cell

The Picture shown in the figure 4.4 gives the basic structure of an Integrated Circuit with package. the legs of a package (VDD and VSS) i.e forming a loop, along with boding wires shown seperately. The major concentration on analysis of orientation of loop which formed with the package legs as discussed and calculation of loop Inductance which represents the stored energy in the form of Magnetic Field , and the radiated energy in the form of radiation resistance.The loop inductance and radiation resistance are calculated using Method of Moments(MoM) and finally analytical expression for loop inductance is formulated using simple approach.

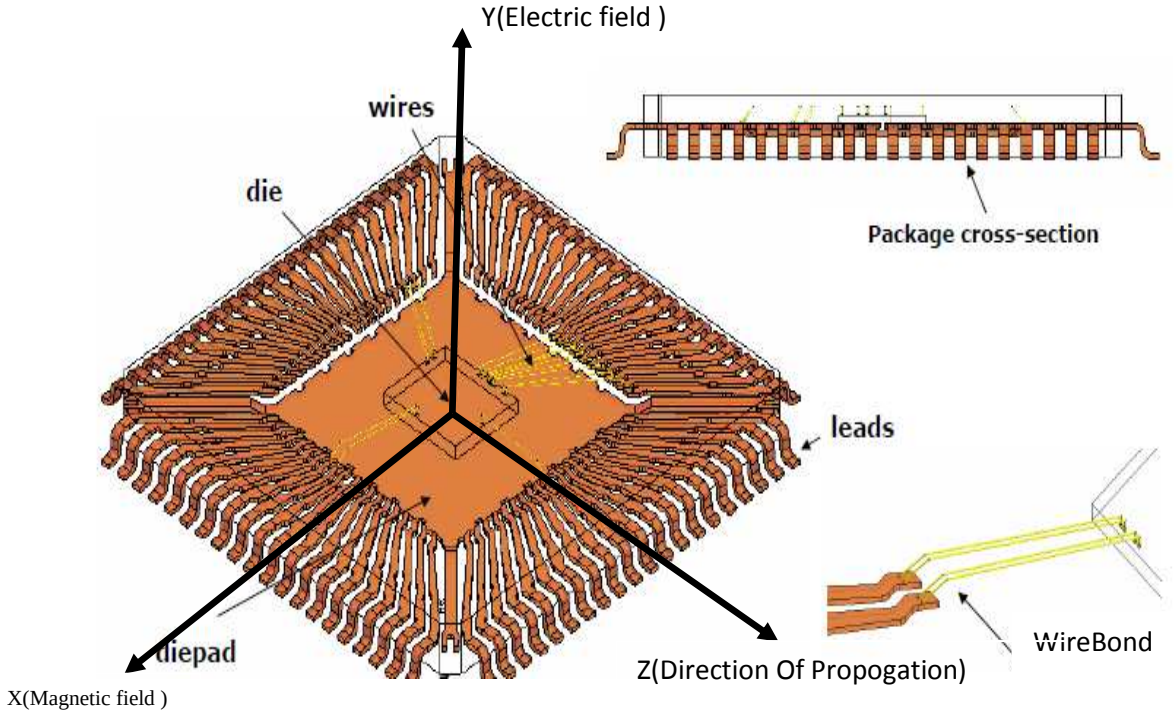

Figure 4.4: Detailed View of DUT

Loop oreintation in TEM cell places a major role in estimating EMI . From the crowford the radiated fied of a magnetic dipole in a TEM cell is given by

$$P_m = \frac{Z_0}{2}\left(\frac{2\pi A}{\lambda_0}\frac{E_0 I_m cos\hat{\phi}}{2V}\right)^2 \qquad (4.1)$$

where $\hat{\phi}$ is the angle between the loop normal and the magnetic field at the source point.

From the Lorentz-reciprocity theorem[10 ch-1], to make the analysis on orientation of loop simpler ,we are applying supply to septum instead of DUT. Consider an empty TEM cell, the electric and magnetic fields looks like as shown in the figure 4.5

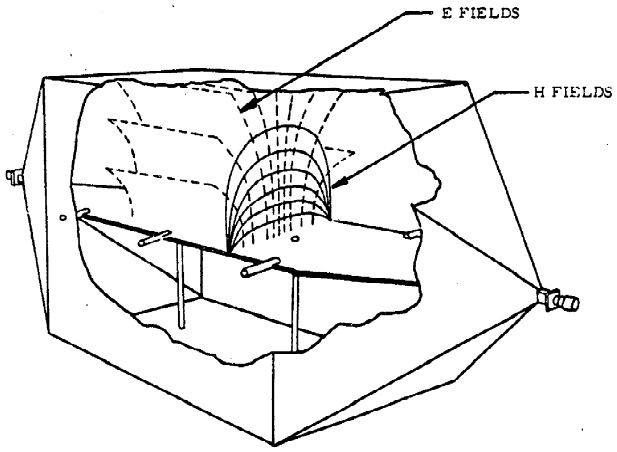

Figure 4.5 : Electric and Magnetic fields of an empty TEM cell

by correlating with the figure 4.4 Detailed view of the DUT ,different orientations of loop in a TEM cell as shown in figure 4.6

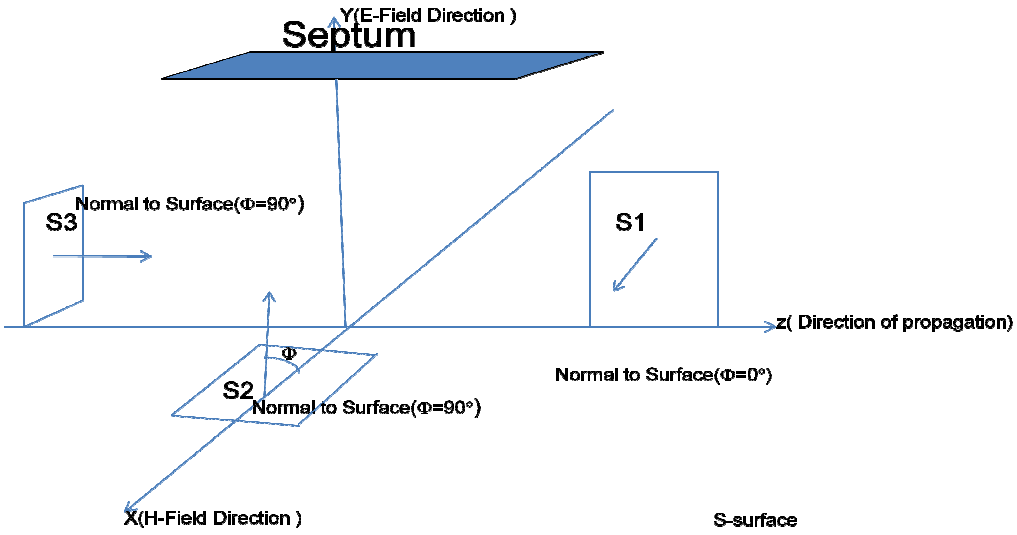

Figure 4.6: Different loop orientations with respect to the Magnetic Field Produced in empty TEM Cell

Consider a loop on yz-plane i.e. S1 surface in figure 4.6. the normal of the loop is in magnetic field (which is produced in an empty cell) direction therefore the angle $\hat{\phi} = 0^0$,which leads to the maximum power carried by the TEM wave. coming to the case surface(S2 in figure4.6) on XZ-plane ,the normal of the surface is perpendicular to the H-field i.e. $\hat{\phi} = 90^0$ means the power carried by the TEM wave is very less and is the same situation with S3 surface which is placed in XY-plane.

To model the equivalent circuit of the loop we require to calculate the loop inductance and radiation resistance, by neglecting the capacitance which is very small for loops. Firstly calculation is done by using Method of Moments (4Nec2 tool) and then by analytical expression for computing inductance and resistance of a loop or multiple loops.

The loop shown in Fig 4.7 represents two leads representing vertically(one supply lead(VDD(dc source)), in EMI point of view acts as a ground and one ground pin i.e. return path) ,along with the bonding wires represents horizontally in which the circle symbol represents current consumption depends on the circuitry connected to IOpad.

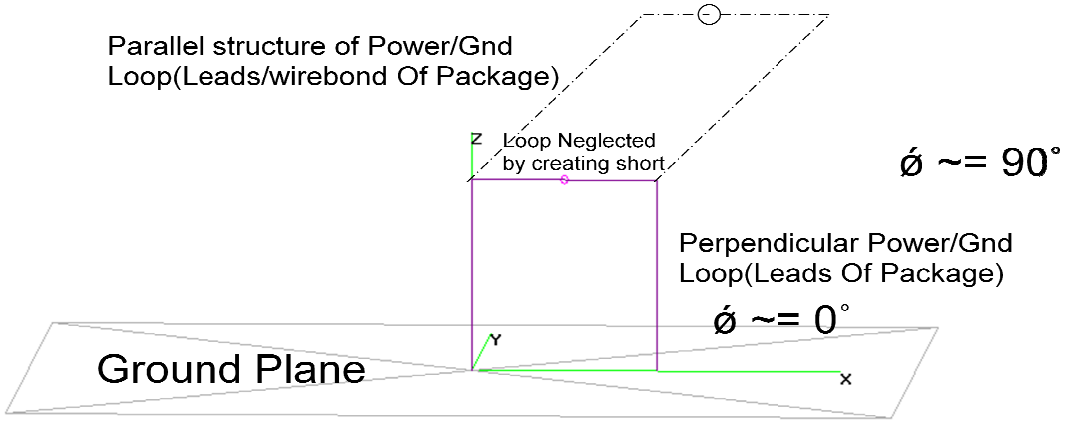

Figure 4.7 Simplified structure of a loop in which the effect of bond wires are replaced by shorting the two leads.

The normal of vertical loop is making an angle 0^0 with the H-field of the septum so this loop contributes more amount of voltage in the septum; the normal of horizontal loop i.e. formed by means of bonding wires makes an angle 90^0 to the H-field of the septum so this loop induces less amount of voltage in the septum. Therefore we have neglected the horizontal loop by short circuiting the vertical loop with the shortest possible path. The problem reduces to a simple rectangular loop, the calculation of inductance and resistance is simple. Firstly we have done using Method of Moments (4Nec2 tool) ,but using this tool have some restrictions ,computation time is more when i feed more number of frequency components ,to eliminate this effect we have used the analytical expression.

4.2 Method of Moments

The task of determining the inductance and resistance is computed by estimating the current distribution in a loop .The task of determining the current distribution on a wire antenna resulting from an arbitrary excitation may be readily stated in terms of an integral equation problem [23]. The formulation begins with the development of an integral expression which defines the electric field resulting from an arbitrary current distribution on the wire. This integral expression will employ a Green's function which relates the electric field at an arbitrary observation point to the current at an arbitrary source point. The integral equation problem then employs the integral expression to relate known electric field boundary conditions to an unknown current distribution on the wire.

The MoM applies orthogonal expansions to translate the integral equation statement into a system of circuit-like simultaneous linear equations. Basis functions are used to expand the current distribution. Testing functions are used to invoke the electric field boundary conditions. Matrix methods are then used to solve for the expansion coefficients associated with the basis functions. The current distribution solution is then constructed from the expansion coefficients. The antenna's radiation characteristics and feed point impedance are then derived from the calculated current distribution.

4.2.1 Pocklington's Integral Equation

A well-known formulation for simple wire antennas is Pocklington's integral equation. Figure 4.8 depicts a representative geometry from which Pocklington's equation can be derived. A simple wire antenna is positioned along the *z* axis in a Cartesian coordinate system. The current is restricted to the centerline of the wire and directed along the *z* axis. Elemental current segments are located at coordinate *z′*. Field observation points are located at coordinates *z*. A feedgap is positioned at *z* = 0. The electric field along the surface of the wire and in the feedgap, which establishes the boundary conditions for the problem, is defined as follows: E_z = 0 on the surface of the wire, $E_z = V_g/\Delta z$ at the feedgap. V_g, the antenna excitation, is normally set to 1.0 volts for input impedance calculations. Δ*z* is commonly set equal the diameter of the wire. However, it is possible to study the impact of feedgap dimensions on antenna input impedance by varying the value of Δ*z*. With the conditions presented in Figure 4.8, Pocklington's equation may be written as Equation 4.2.

$$\int_{-\frac{l}{2}}^{\frac{l}{2}} I(z') \left[\frac{\partial^2}{\partial z^2} + k^2\right] \frac{e^{-jkR}}{4\pi R} dz' = j\omega\varepsilon E_z(z) \qquad (4.2)$$

where $R = \sqrt{\rho^2 + (z - z')^2}$

The variable *R* represents the distance between the current source and field observation points. The variable ρ specifies the radius of the wire. The current distribution $I_z(z')$ is defined along the length of the wire from $z' = l/2$ to $z' = -l/2$. The kernel $[\partial^2/\partial z^2 + k^2]$ denotes the wave equation differential operator on the free space Green's function $e^{-jkR}/4\pi R$. The constant *k* specifies the free space wave number. $E_z(z)$ represents the electric field generated by the current on the wire. With a specific excitation applied, as modeled through the appropriate boundary conditions, radiation characteristics and feedpoint impedances are determined from knowledge of the

antenna's current distribution $I^z(z')$. Of the many techniques available to solve such integral equation problems, the Method of Moments is one of the industry's more popular approaches.

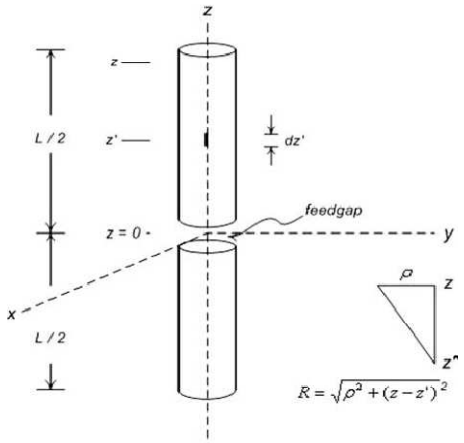

Figure 4.8 : Integral equation formulation

4.2.2 The Method of Moments

The fundamental concept behind the MoM employs orthogonal expansions and linear algebra to reduce the integral equation problem to a system of simultaneous linear equations. This is accomplished by defining the unknown current distribution $I_z(z')$ in terms of an orthogonal set of "basis" functions and invoking the boundary conditions—the values of the electric field on the surface of the wire and in the feedgap—through the use of an inner product formulation. This inner product operation employs an orthogonal set of "testing" functions to enforce the boundary conditions, in an average sense, along the surface of the wire and in the feed gap. Moving the current's expansion coefficients to the outside of the integro-differential Operator permits the evaluation of known functions, yielding values which are loosely defined as impedances. The current's expansion coefficients, the orthogonal projections of the electric field boundary conditions, and these so-called impedances are gathered into a system of simultaneous linear equations. This system of equations is solved to yield the current's expansion coefficients. The original current distribution is then determined by introducing these coefficients back into the basis function expansion. The solution procedure begins by defining the unknown current distribution $I_z(z')$ in terms of an orthogonal set of basis functions. Two categories of basis functions exist. Sub-domain basis functions, significantly more popular in industry, subdivide the wire into small segments and model the current distribution on each segment by a simple geometrical construct, such as a

rectangle, triangle, or sinusoidal arc. The amplitudes of these constructs represent the expansion function coefficients.

These simple constructs, illustrated in Figure 4.9, often overlap to maintain continuity of the current distribution along the wire. Entire domain basis functions employ a more formal orthogonal expansion, such as a Fourier series, to represent the current distribution along the entire wire. Entire domain basis functions tend to yield more complicated calculations for the so-called impedances and, therefore, are less popular. The introduction of the re-defined current distribution reduces the integral equation to the form.

$$\sum_{n=1}^{N} C_n G_n(z) = E_z(z) \tag{4.3}$$

Where

$$G_n(z) = \frac{1}{j4\pi\omega\varepsilon} \int_{-\frac{l}{2}}^{\frac{l}{2}} F_n(z') \left[\frac{\partial^2}{\partial z^2} + k^2\right] \frac{e^{-jkR}}{R} dz'$$

C_n=current's expansion coefficient

$F_n(z')$=basis function

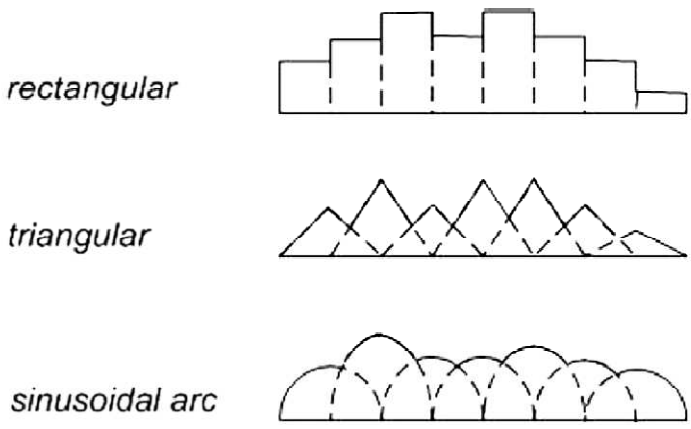

Figure 4.9: Typical basis function

The boundary conditions are now enforced through the use of an inner product operator with a set of orthogonal testing functions. Each testing function is applied to both sides of the integral equation, the inner product then enforces the boundary condition at the location described by the testing function. This operation may be thought of as simply enforcing the boundary condition at a single point on the wire. After each testing function operation, the integral equation will appear as Equations 4.4 and 4.5.

$$\sum_{n=1}^{N} C_n < H_m(z), G_n(z) > = < H_m(z), E_z(z) > \quad (4.4)$$

Where < > represents the inner product operator.

$$< H_m(z), E_z(z) > = \int_{-\frac{l}{2}}^{\frac{l}{2}} H_m(z) G_n(z)\, dz$$

Where $H_m(z)$ is a testing function which has a non-zero value for only a small segment of wire located at $z = z_m$. There are two common approaches to formulating the orthogonal set of testing functions. The first approach, the point matching or co-location technique, defines the testing function in terms of Dirac delta functions (Eq. 4.5).

$$H_m(z) = \delta(z - z_m) \quad (4.5)$$

Where z_m are specific points on the wire at which the boundary conditions are enforced. The z_m are usually selected to correspond with the midpoint of each basis function. The second approach, Galerkin's technique, defines the testing function to be the same as the basis Function. Galerkin's technique, although more complicated from a computational perspective, enforces the boundary condition more rigorously than the point matching technique. However, this more rigorous approach is seldom required for simple wire antenna problems.

The entire boundary condition is enforced by applying the complete set of testing functions. This operation yields a set of integral equations.

$$[Z_{mn}][I_n] = [V_m] \quad (4.6)$$

where $Z_{mn} = \int_{-\frac{l}{2}}^{\frac{l}{2}} H_m(z) G_n(z)\, dz$

$I_n = C_n$

$V_{mn} = \int_{-\frac{l}{2}}^{\frac{l}{2}} H_m(z) E_n(z)\, dz$

This circuit-like set of simultaneous linear equations will yield the value of C_n.

$$[I_n] = [Z_{mn}]^{-1}[V_m] \quad (4.7)$$

The validity of the assumptions introduced into MoM type formulations are established through empirical means. The codes incorporating these formulations are run for a large number of test cases with the results compared to experimental observation. Certain topics have received significant attention in the literature: the current distribution on the wire (the "thin wire approximation"), the orthogonality and completeness of the basis and testing functions, the modeling of the feed point excitation, the numerical

evaluation of Z_{mn}, and the solution technique which yields C_n from the set of simultaneous linear equations. Although some of the assumptions continue to attract attention from a mathematically rigorous perspective, the codes incorporating them have been thoroughly exercised and deemed suitable for antenna engineering applications. The most well-known of the codes using the MoM is the Numerical Electromagnetics Code (NEC), which is widely used to solve problems that can be defined as sets of one or more "wires" (linear elements).The procedure to construct the required geometry are discussed in appendix-2 and detailed in [7] ,calculate the inductance and resistance.

For a loop with dimensions of 1mm length and 0.5mm width on the ground plane

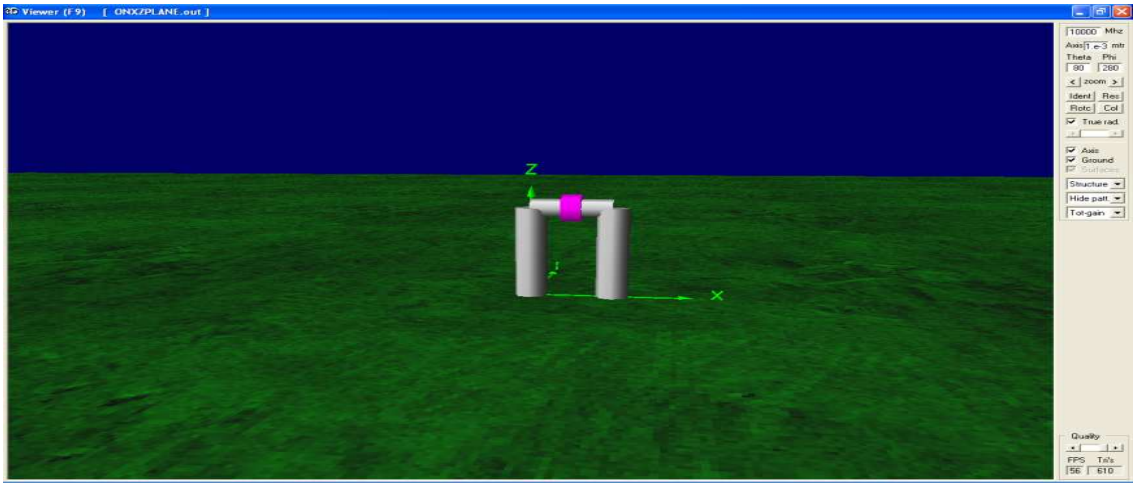

(a)

Its inductance computed in 4nec2 tool is

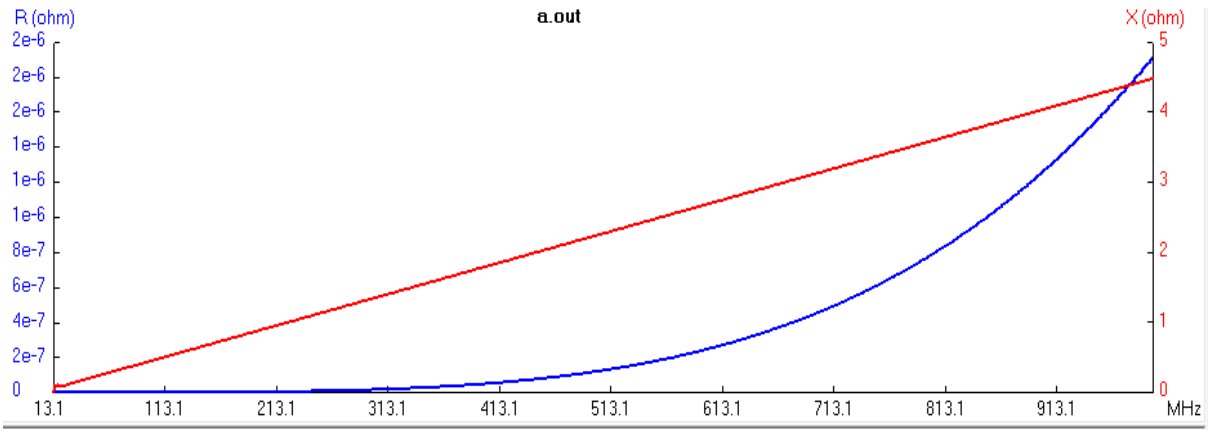

(b)

Figure 4.10: (a) loop on ground plane with dimensions of 1mm length and 0.5mm width and (b) loop inductance and resistance computed in MoM

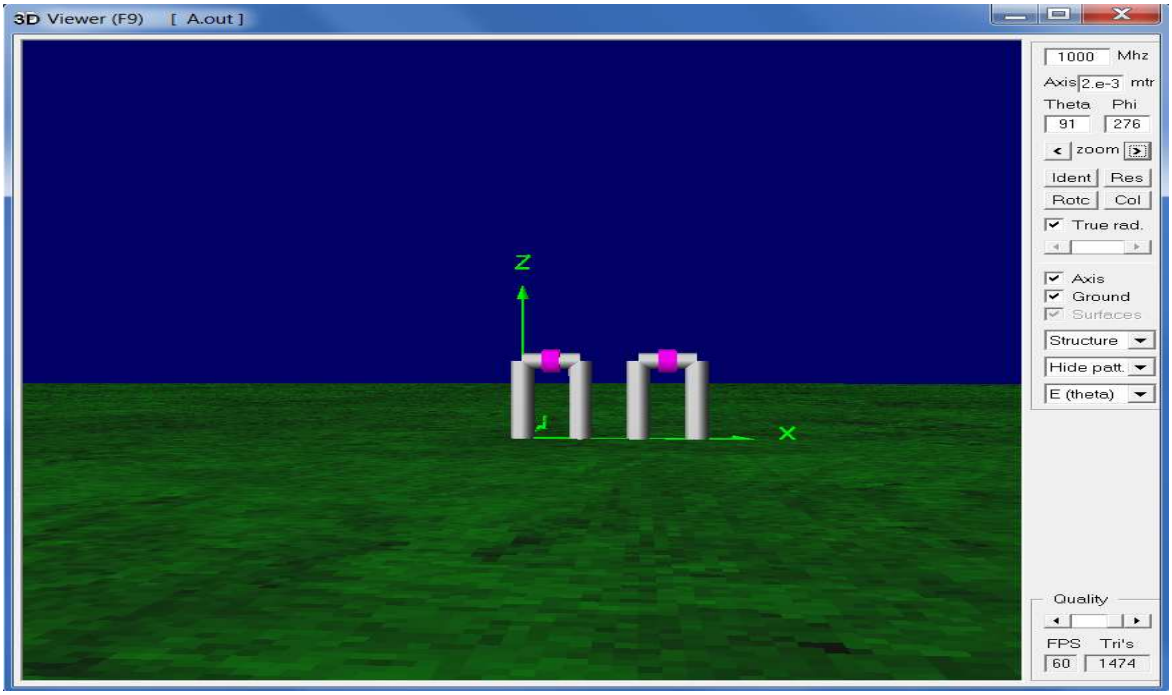

(a)

Its inductance computed for two loops separated at a distance of 5mm , computed in tool is

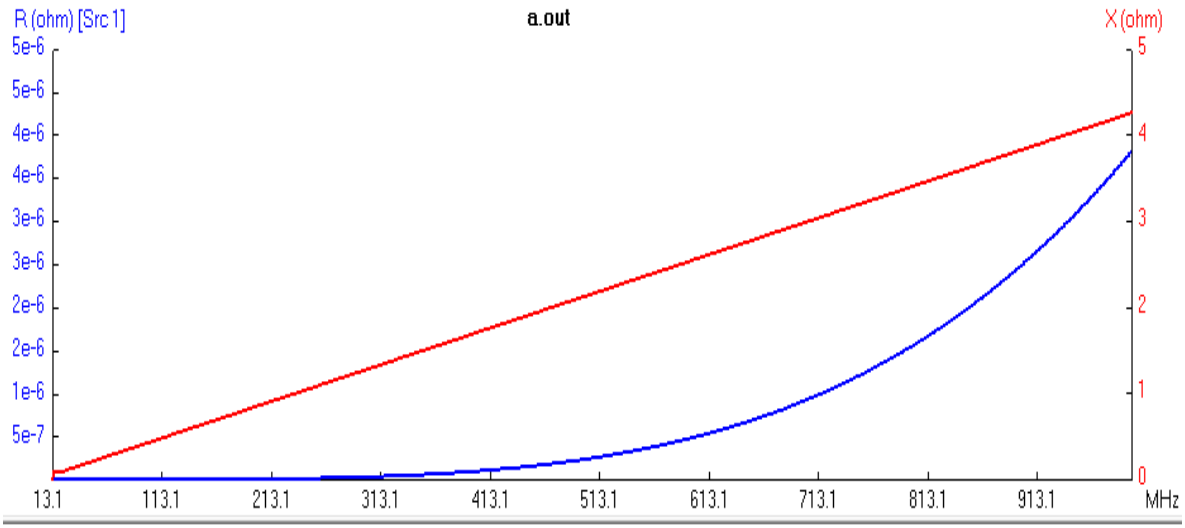

(b)

Figure 4.11: (a) two loops on ground plane with dimensions of 1mm length and 0.5mm width separated with 0.5mm and (b) loop inductance and resistance computed in MoM

4.3 Analytical Expression

Self inductance of a straight cylindrical wire: Let AB be a length l of a cylindrical wire of radius ρ transverse by current i distributed uniformly over the cross section of the wire as shown in Figure 4.12 .

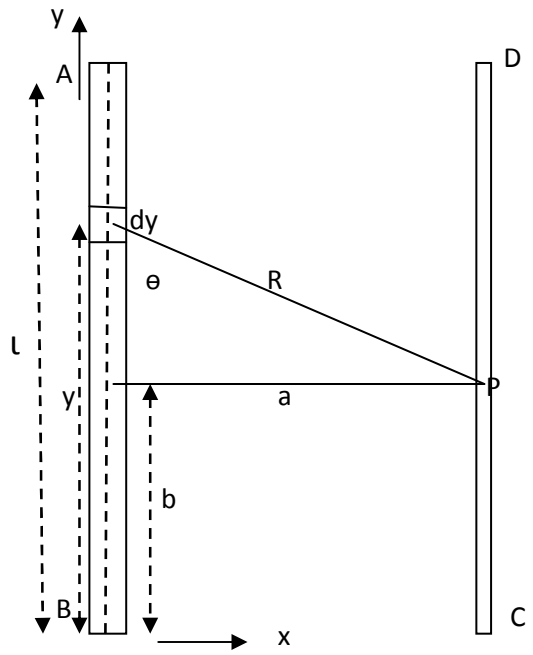

Figure 4.12 : A wire of length ℓ in which dy is a small element ,p is an arbitrary point at a distance R from element to calculate force .

The magnetic force at P nomal to the paper due to the element of the cylinder of length dy is calculated using biot-sarvart's law

$$dH = \frac{Idl \times \bar{R}}{4\pi R^3} \qquad (4.8)$$

Where R is the distance between element dy and point of observation P

$$i\frac{dy}{R^2}sin\theta = \frac{ia\,dy}{[a^2 + (y - b^2)]^{\frac{3}{2}}} \qquad (4.9)$$

It is easy to show that the force at any point outside a right cylinder is the same as though the current were concentrated at the axis of the wire . The force at P due to the whole length of the cylinder carrying unit current is calculated using integrating through out the length l as shown in Equ (4.10)

$$H = \frac{1}{4\pi}\int_0^l \frac{ia\,dy}{[a^2 + (y - b^2)]^{\frac{3}{2}}} = \frac{1}{4\pi}\left[\frac{l-b}{a\sqrt{a^2 + (l-b)^2}} + \frac{b}{a\sqrt{a^2 + b^2}}\right] \qquad (4.10)$$

The voltage in terms of electric field as Equ (4.11)

$$V = \int E.dy \;\; = \int_S \nabla \times E.dS$$

$$= \int_S -\frac{\partial B}{\partial t}.dS = -\frac{\partial}{\partial t}\int_S B.dS \qquad (4.11)$$

Voltage across an Inductor is

$$V = L\frac{di}{dt} = \frac{d}{dt}(Li) \qquad (4.12)$$

From (4.11) and (4.12)

$$Li = \int_S B.dS \qquad (4.13)$$

$$L = \frac{\mu}{i}\int_S H.dS = \frac{\mu}{i}\int_S H.dxdy \qquad (4.14)$$

Where L is the Inductance and 'i' is the current flowing through the inductance

The number of lines of magnetic force dN, with in the strip CD .of breadth dx , is found by integrating the expression for H along the strip.

Thus,

$$dN = \frac{dx}{a}\int_0^l \frac{1}{4\pi}\left[\frac{l-b}{a\sqrt{a^2+(l-b)^2}} + \frac{b}{a\sqrt{a^2+b^2}}\right]dy$$

$$= \frac{2dx}{4\pi a}\left[\sqrt{a^2+l^2} - a\right] \qquad (4.15)$$

The Whole number of lines of force N outside the wire which will collapse upon the wire when the current ceases is found by integrating dN with respect to x from x=ρ to x=∞.Thus Replacing a by x in

$$N = 2\int_\rho^\infty \frac{1}{4\pi}\left[\frac{\sqrt{x^2+l^2}}{x} - I\right]dx$$

$$= \frac{2}{4\pi}\left[\sqrt{x^2+l^2} - x - l\,log\frac{\sqrt{x^2+l^2}+l}{x}\right]_\rho^\infty \qquad (4.16)$$

Or $$N = \frac{2}{4\pi}\left[l\,log\frac{\sqrt{\rho^2+l^2}+l}{\rho} - \sqrt{\rho^2+l^2} + \rho\right]$$

$$= \frac{2l}{4\pi}\left[log\frac{2l}{\rho} - I\right]\; approximately \qquad (4.17)$$

This is the number of lines of force outside the wire due to unit current in the wire is given by Equ (4.17), and is therefore that part of its self-inductance L_1 due to the external-field.

$$L_1 = \frac{2\mu}{4\pi}\left[l\, log \frac{\sqrt{\rho^2 + l^2} + l}{\rho} - \sqrt{\rho^2 + l^2} + \rho \right] \tag{4.18}$$

We must now find L_2 due to the field within wire .

The strength of field at the point P within the wire is $\frac{2ix}{\rho^2}$. The number of lines of force in the length l with in the element dx is there fore

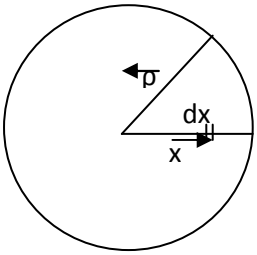

$$dN = \frac{2ilxdx}{\rho^2} \tag{4.19}$$

Figure 4.13: cross section of a wire

If we integrate this expression (4.19) from 0 to ρ we have the whole number of lines of force within the conductor. Therefore

$$N = \frac{li}{\rho^2}\int_0^{\rho} 2xdx = li \tag{4.20}$$

Thus there are i lines or tubes per unit of length within any cylindrical conductor carrying a current I , or one tube per cm for unit current.

The lines within conductor do not cut the whole cross section of the conductor, as do those without. We must weight them, in estimating their effect on the self-inductance, in proportion to the area of the section of the conductor cut by each elementary-tube.

$$iL_2 = l\int_0^{\rho} \frac{2ix}{\rho^2}.\frac{x^2}{\rho^2}dx = l\left[\frac{i}{2}.\frac{x^4}{\rho^4}\right]_0^d = \frac{li}{2} \tag{4.21}$$

$$iL_2 = \frac{l}{2} \tag{4.22}$$

Thus the l lines or tubes within the conductor contribute only half as much toward the self inductance of the conductor as an equal number of lines outside the conductor would do .If the permeability of the wire is μ the part of the self-inductance due to the internal field is

$$L_2 = \frac{\mu}{4\pi} * \frac{l}{2} \tag{4.23}$$

The field at P is

$$H = \frac{2ix}{\rho^2} \tag{4.24}$$

The total self inductance of the length l of straight wire is therefore the sum of L_1 and L_2 .

$$L = 2\frac{\mu}{4\pi}\left[l\, log \frac{\sqrt{\rho^2+l^2}+l}{\rho} - \sqrt{\rho^2+l^2} + \rho + \frac{l}{4}\right] \tag{4.25}$$

The mutual inductance of two parallel wires of length l, radius ρ and distance apart d will be the number of lines of force due to unit current in one which cut the other when the current disappears . This will be the value of N given by (2A) when the limits of integration are d and ∞ instead of ρ and ∞ as before

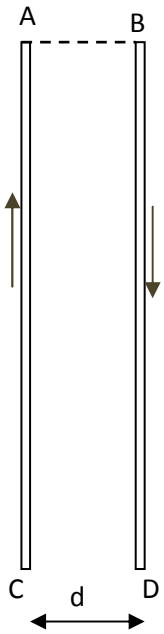

Figure 4.14: Two parallel wires separated by d distance

$$M = 2\frac{\mu}{4\pi}\int_d^\infty \left[\frac{\sqrt{x^2+l^2}}{x} - I\right]dx = 2\frac{\mu}{4\pi}\left[\sqrt{x^2+l^2} - x - l\, log\frac{\sqrt{x^2+l^2}+l}{x}\right]_d^\infty$$

$$M = 2\frac{\mu}{4\pi}\left[l\, log \frac{\sqrt{d^2+l^2}+l}{d} - \sqrt{d^2+l^2} + d\right] \tag{4.26}$$

Equation 4.26 which is an exact expression when the wires have no appreciable cross section , is not an exact expression for the mutual inductance of two parallel cylindrical wires, but is not appreciably in error even when the section is large and d is small if l is great compared with d .

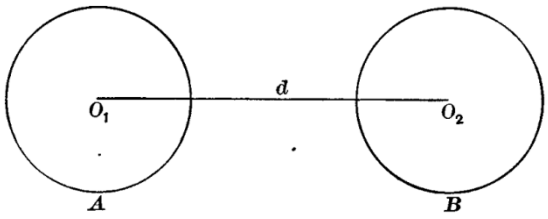

The force in that case due to A at all points outside A is exactly the same as though the current were concentrated at the center O_1 of A; and the geometrical mean distance from O1 to the cross section of B is exactly the distance d between O1 and O2. The mean distance from O1 to all the points in the section of B is not , however ,quiet the

same as d , although the mean of the log of these distances is logd .Hence there is a very slight difference in the last term of (12) depending upon the section of the wires and a still smaller difference in the other terms. This is however , too small to be appreciable in any ordinary case, being a small quantity of the second order when l is large compared with d.

Self Inductance of a Rectangle:

The self-inductance of the rectangle of length a and breadth b as shown in Fig:4.15

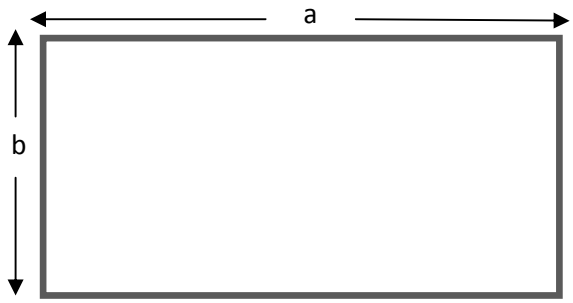

Figure 4.15*:* Rectangular loop with dimensions a and b.

$$L = 2(L_a + L_b - M_a - M_b) \tag{4.27}$$

where L_a and L_b are the self-inductances of the two sides of length a and b taken alone , M_a and M_b are the mutual inductances of the two opposite pairs of length a and b ,respectively.

From (4.25) and (4.26) we therefore have ,The Inductance of the Rectangle is computed by

$$L_a = 2\frac{\mu}{4\pi}\left[a\, log\frac{\sqrt{\rho^2 + a^2} + a}{\rho} - \sqrt{\rho^2 + a^2} + \rho + \frac{a}{4}\right] \tag{4.28}$$

$$L_b = 2\frac{\mu}{4\pi}\left[b\, log\frac{\sqrt{\rho^2 + b^2} + b}{\rho} - \sqrt{\rho^2 + b^2} + \rho + \frac{b}{4}\right] \tag{4.29}$$

$$M_a = 2\frac{\mu}{4\pi}\left[a\, log\frac{\sqrt{b^2 + a^2} + a}{b} - \sqrt{b^2 + a^2} + b\right] \tag{4.30}$$

$$M_b = 2\frac{\mu}{4\pi}\left[b\, log\frac{\sqrt{b^2 + a^2} + b}{a} - \sqrt{b^2 + a^2} + a\right] \tag{4.31}$$

By substuting (4.28),(4.29),(4.30) and (4.31) in (4.27)

$$L = 4\frac{\mu}{4\pi}\left[a\,log\frac{\sqrt{\rho^2+a^2}+a}{\rho} - \sqrt{\rho^2+a^2} + \rho + \frac{a}{4} + b\,log\frac{\sqrt{\rho^2+b^2}+b}{\rho} \right.$$
$$- \sqrt{\rho^2+b^2} + \rho + \frac{b}{4} - \left(a\,log\frac{\sqrt{b^2+a^2}+a}{b} - \sqrt{b^2+a^2} + b \right)$$
$$\left. - \left(b\,log\frac{\sqrt{b^2+a^2}+b}{a} - \sqrt{b^2+a^2} + a \right) \right] \qquad (4.32)$$

Inductance on a ground plane:

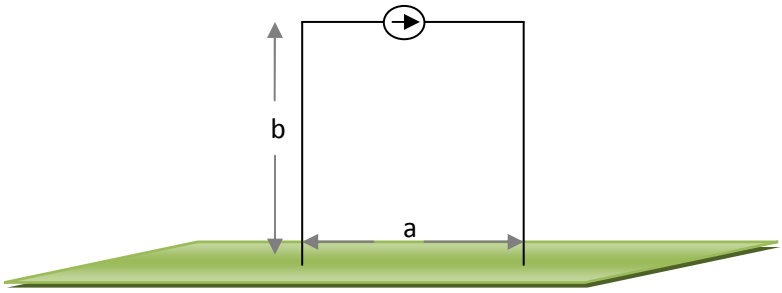

Figure 4.16: Loop located on a ground plane

Now to calculate the inductance on a ground plane. which can be done by using Method Of Images, The Method of Images is closely akin to the reflection principle except that here we are concerned with replacing a source within a given boundary by a system of sources, which are images of the original source in the boundary .replicating the loop and changing the direction of current, can remove the ground. now the problem has become a simple loop.

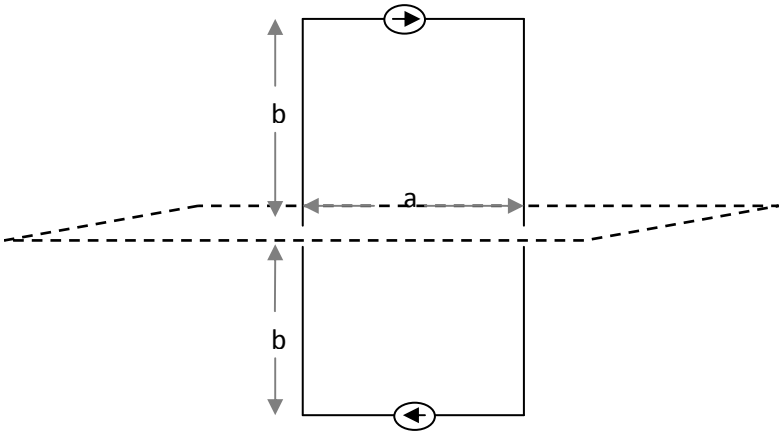

Figure 4.17: Equivalent loop by replicating to remove ground using image theory

Now the loop vertical length has increased by two times by applying method of images. Using the above stated formulae calculate the inductance and finally reducing to half gives the equivalent inductance of loop on ground plane.

Inductance of Multiple Loops:

Considering the multiple loops, in which a1, b1 are dimensions of first loop and a2,b2 are dimensions of second loop, d is the distance between two loops.

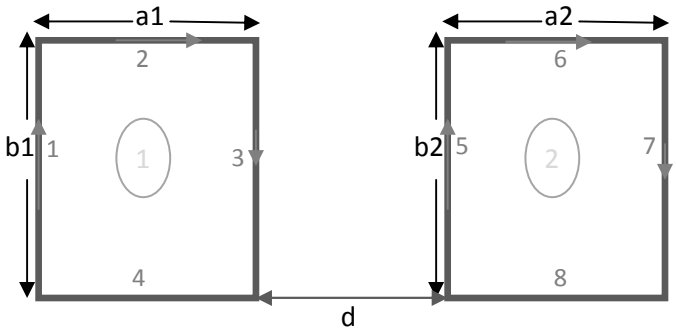

Figure 4.18: Multiple loops with distance between loops as d.

1,2,3,4 are the segments of first loop and 5,6,7,8 are the segments of second loop, then the inductance of loop1 is inductance of segment 1 $L_1 = (L_{11} - M_{13} + M_{15} - M_{17})$ where L_{11} is the self inductance of segment 1 ,M_{13} is the mutual inductance between segment 1 and 3 , the current direction in both segments are opposite that is why, the mutual inductance is deducted from L_{11} , M_{15} is the mutual inductance between segment 1 and 5 , the current direction in both segments are same that is why the mutual inductance is added to L_{11} in the same way all the segments are calculated.

inductance of segment 2 $L_2 = (L_{22} - M_{24})$

inductance of segment 3 $L_3 = (L_{33} - M_{31} - M_{35} + M_{37})$

inductance of segment 4 $L_4 = (L_{44} - M_{42})$

Total inductance of first loop is $\boldsymbol{L1 = L_1 + L_2 + L_3 + L_4}$

The inductance of the second loop is

inductance of segment 5 is $L_5 = (L_{55} - M_{57} - M_{53} + M_{51})$

inductance of segment 6 is $L_6 = (L_{66} - M_{68})$

inductance of segment 7 is $L_7 = (L_{77} - M_{75} + M_{73} - M_{71})$

inductance of segment 8 $L_8 = (L_{88} - M_{86})$

Total inductance of second loop is $\boldsymbol{L2 = L_5 + L_6 + L_7 + L_8}$

Total inductance is L1+L2.

This procedure can be used to calculate the inductance of multiple loops.

The inductance of a loop computed using analytical expression for one loop shown in the figure 4.19, the plot shown is by eliminating the self inductance due to internal field .

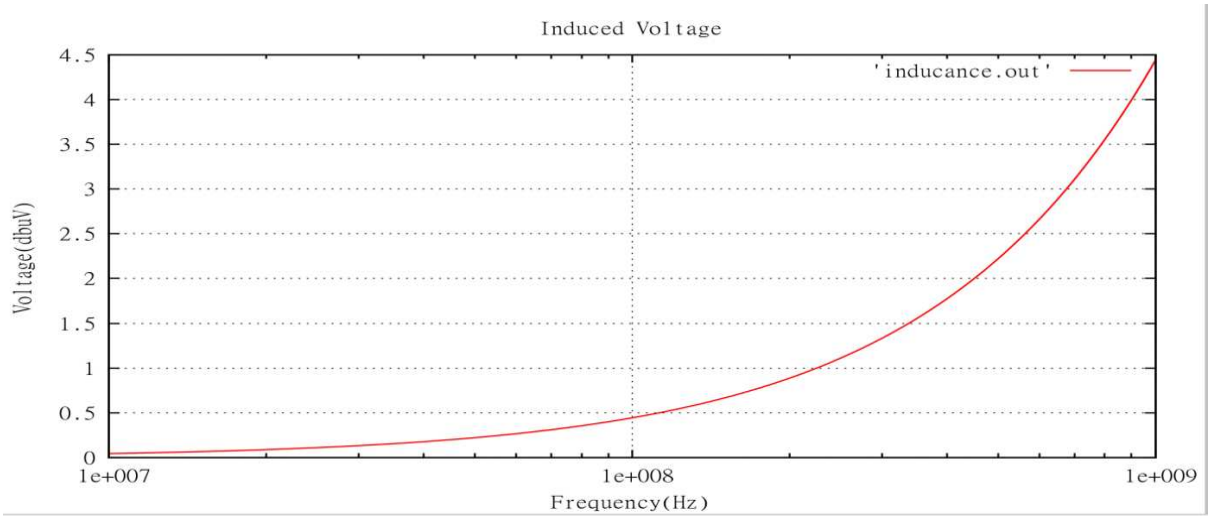

(a)

For two loops :

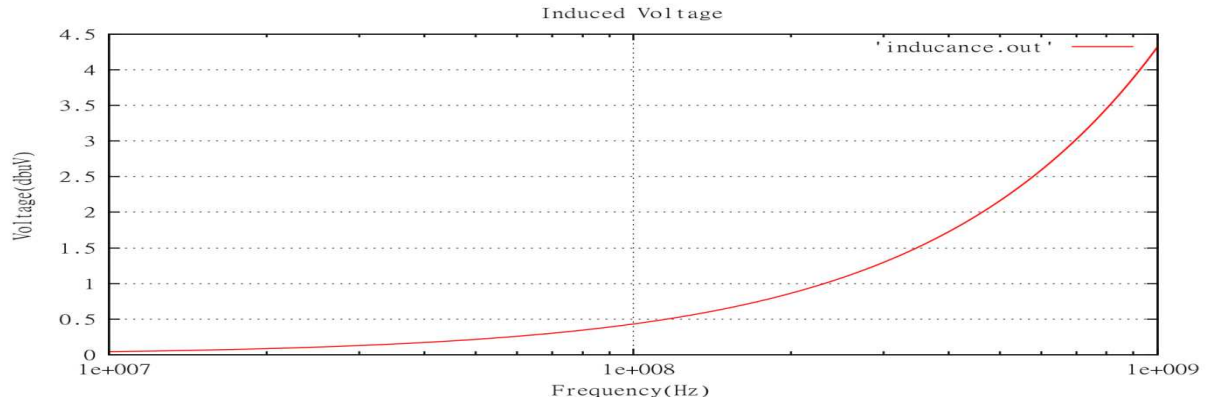

(b)

Figure 4.19 (a) inductance of one loop computed using analytical expression (b) inductance of two loops computed using analytical expression.

Radiation Resistance :

The radiation resistance of a loop is a well known expression (4.33) []

$$R = 320\,\pi^4 \left(\frac{S^2}{\lambda^4}\right) \qquad (4.33)$$

Where S is a surface area i.e. S=a×b

λ is a wave length

The loop on ground is calculated by applying image theory as done for inductance

Then the area S is 2a×b, finally the R is made half then

$$R = 160\,\pi^4 \left(\frac{(2a \times b)^2}{\lambda^4}\right) \tag{4.34}$$

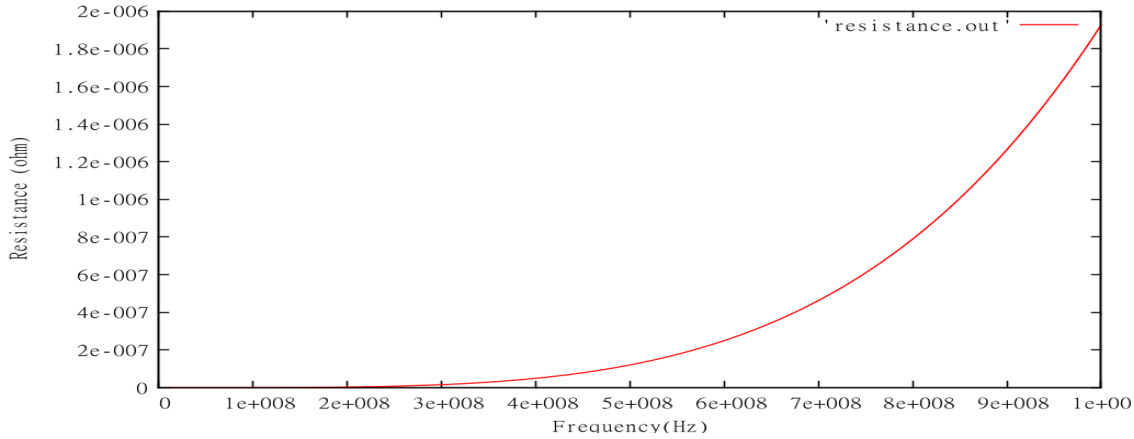

Figure 4.20 : resistance of the loop computed using the analytical expression.

The above results are in good correlation with the results computed using MoM(4Nec2 tool).

5. UNIFIED ELECTROMAGNETIC MODEL

5.1 Unified Model of a TEM Cell with Loaded DUT :

Using (3.36), (3.5), ($Z_o = \sqrt{\frac{L}{C}}$), the TEM cell can be equivalently replaced with the circuit parameter. Fig.5.1 is illustrating the TEM cell equivalent circuit model terminated with the characteristic impedance along with the DUT as excitation source the excitation source of the TEM cell is the IC's package pins and bonding wire. Using chapter 4, the excitation source which is the package pins and bond wire, can be modelled and coupled to the TEM cell.

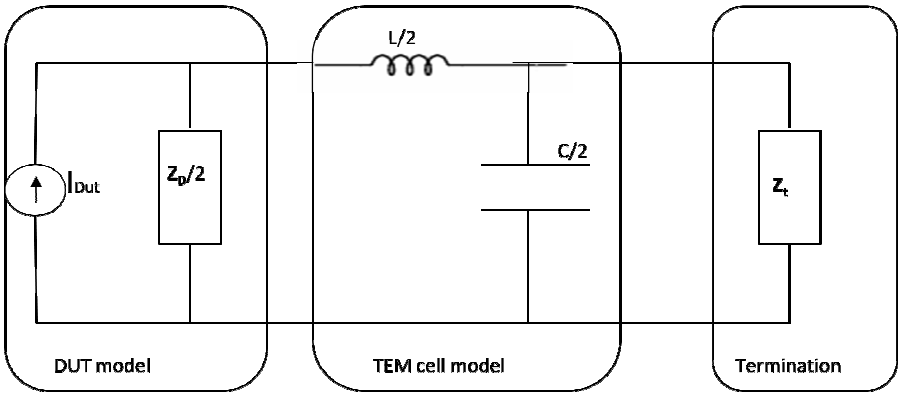

Figure 5.1: Complete model of TEM cell terminated with the characteristic impedance coupled with the DUT model as excitation source.

Where I_{Dut} is the current profile either in Time Domain or Frequency Domain , Z_D is the loop impedance simulated using MoM or analytical expression , L and C are inductance and Capacitance resp. of the TEM cell calculated using Conformal Mapping multiple times the effective length of the TEM cell. Z_t is the Terminating impedance of a TEM cell. Z_D is made half because as the TEM cell is terminated on both sides with its characteristic impedance, i.e. one side is directly terminated and other with a coaxial line, so half the voltage induced flows to the termination and only half is measured in Spectrum analyser .

5.2 Tool Flow:

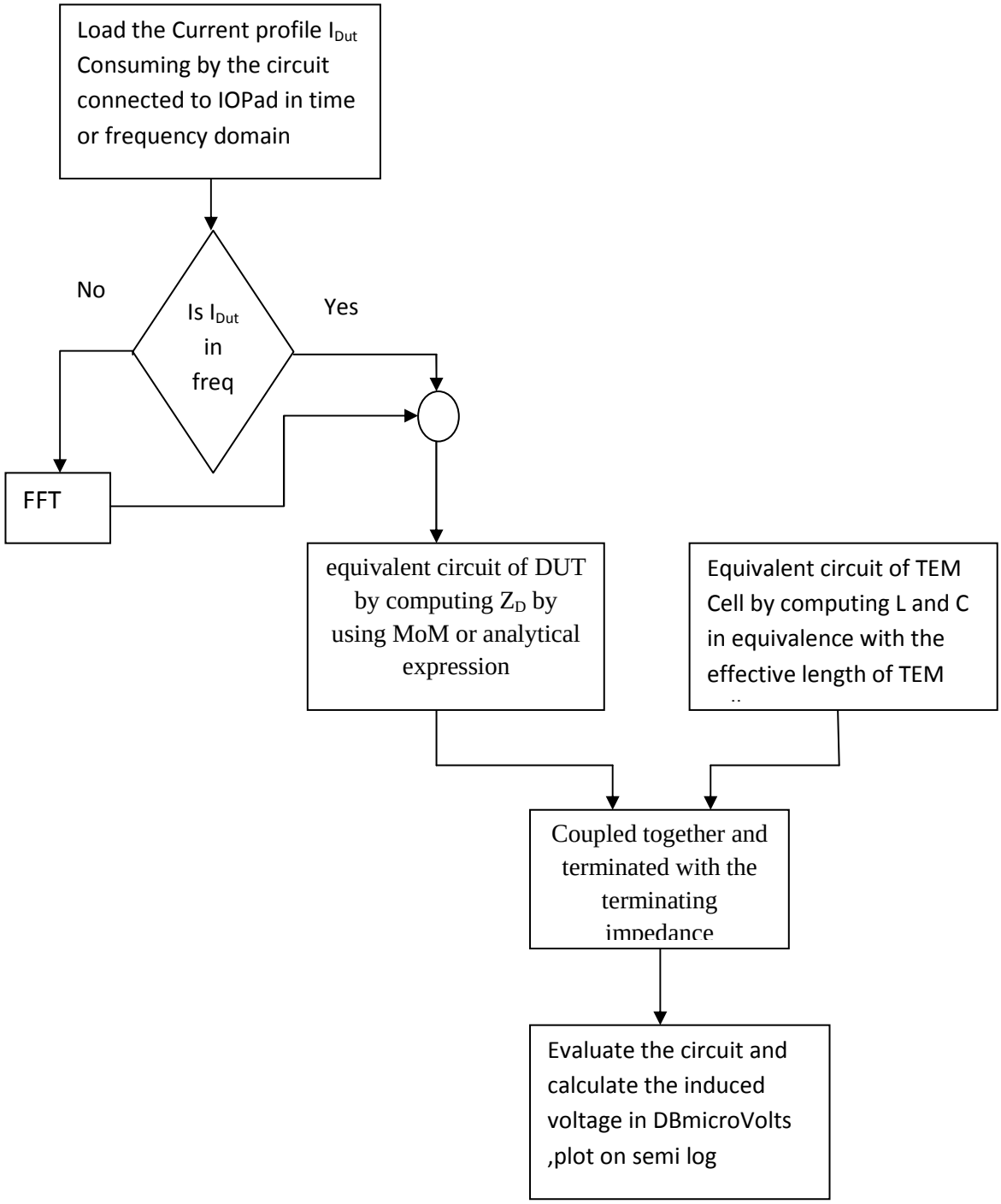

Figure 5.2:Complete flow of the tool.

5.2 Simulation Results :

Computed using MoM: Here MoM is used for analysis of different structures, in order to reduce the radiated emission. using MoM we have started the frequency from 10MHz because of the limitation of 4Nec2 tool .

first loop of dimension 1mm length ,1mm width with a separation between them 0.5mm (normal dimensions of IC package)

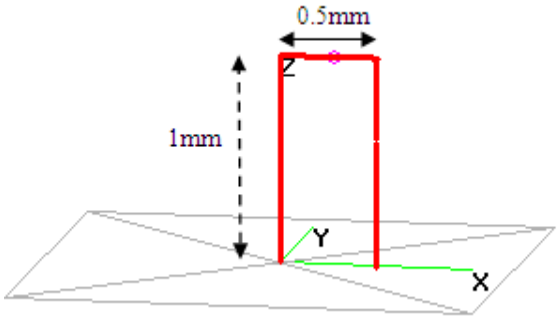

(a) loop 1mm-0.5mm-1mm

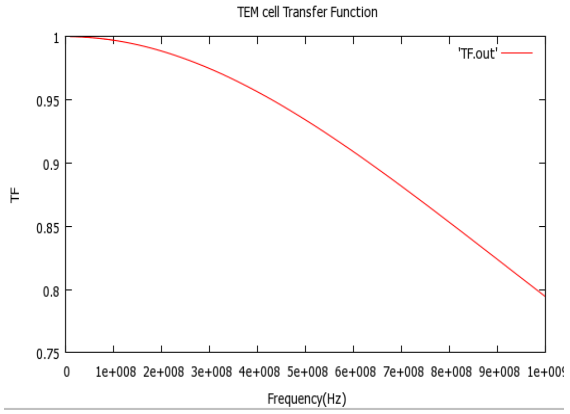

(b) TEM cell Transfer Function

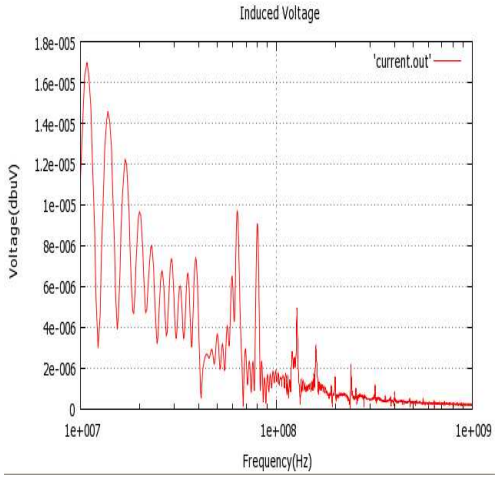

(c) Current profile in frequency domain

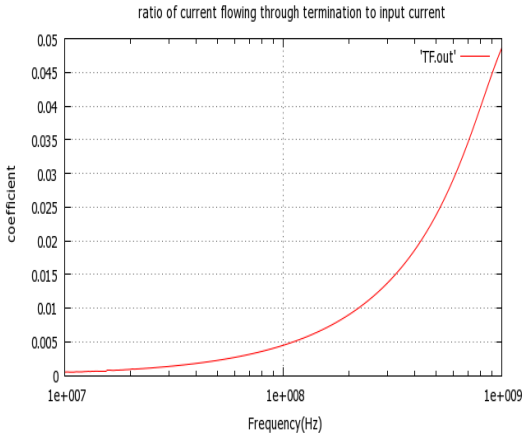

(d) plot of ratio of current through termination to input current

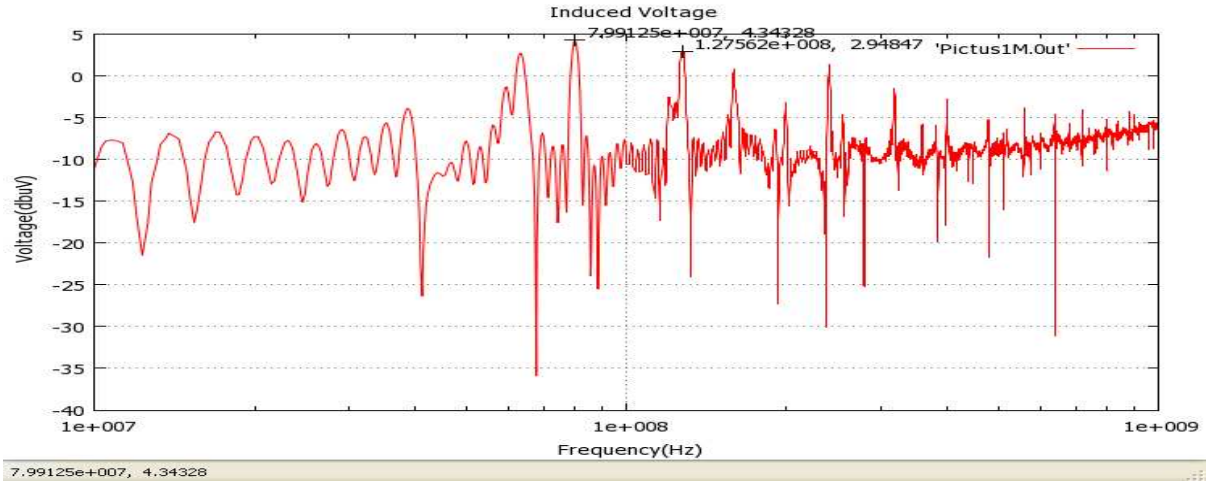

(e) Induced voltage of loop 1mm-0.5mm-1mm

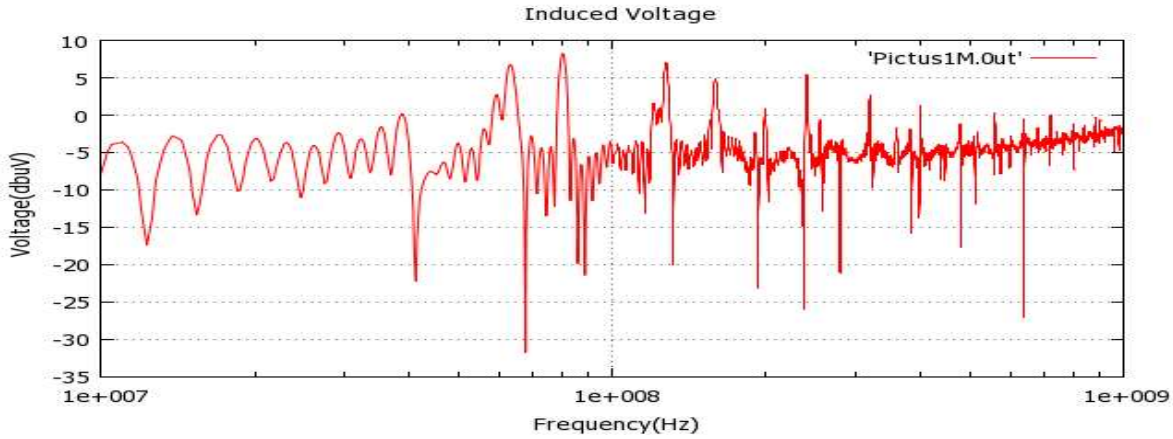

(f) Induced voltage of loop 1mm -1mm-1mm

Figure 5.3:Analysis of loop having dimensions 1mm length ,1mm width with a separation between them 0.5mm using MoM

Secondly it is done by reducing the ground plane to half

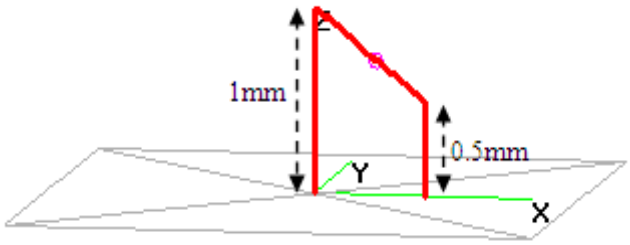

(a) loop formed by reducing length of ground to half

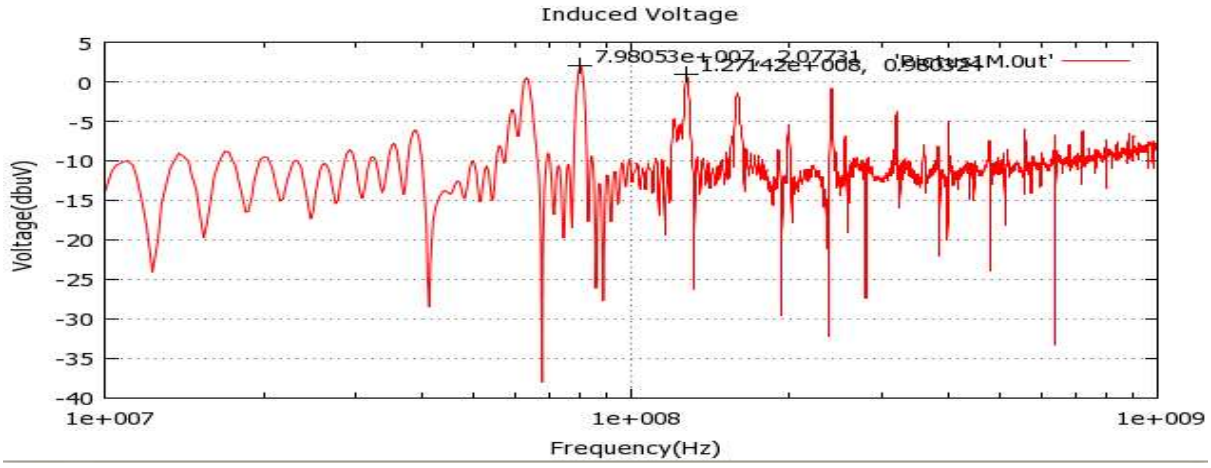

(b) induced voltage of loop formed by reducing ground length

Figure 5.4: Analysis of loop in which ground leg is reduced to half ,in which DUT is modelled using MoM

If two loops are present in same direction

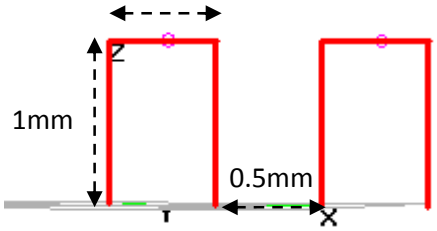

(a)Two loops separated with 0.5mm

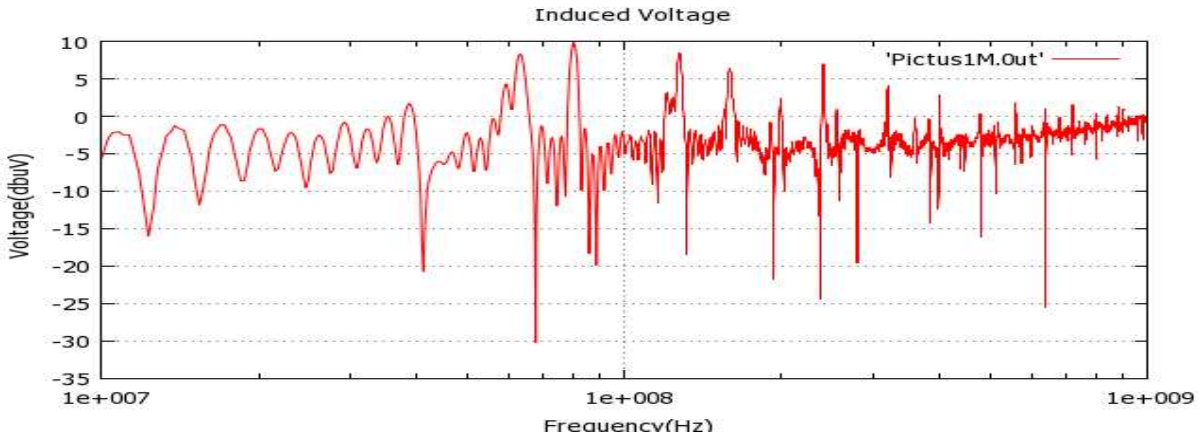

(b) induced voltage formed for two loops separated with 0.5mm ,

Figure 5.5: Analysis of Two loop separated with 0.5mm ,DUT modelled using MoM

By using Analytical Expression : First to correlate with the above results inductance is computed by excluding the self-inductance caused due to internal field.(all loops are of dimensions 1mm length , separated by 0.5mm width)

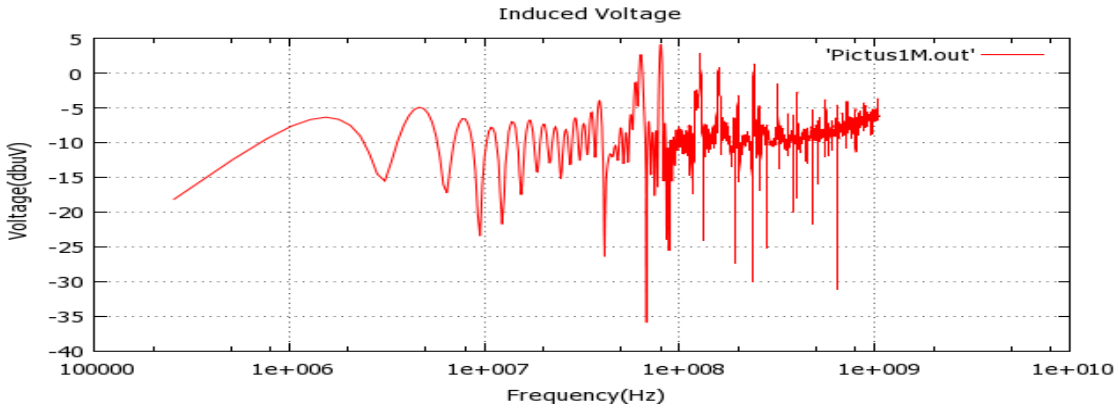

(a) Induced voltage computed by excluding the self-inductance caused due to internal field.

induced voltage computed by including the self-inductance caused by internal field:

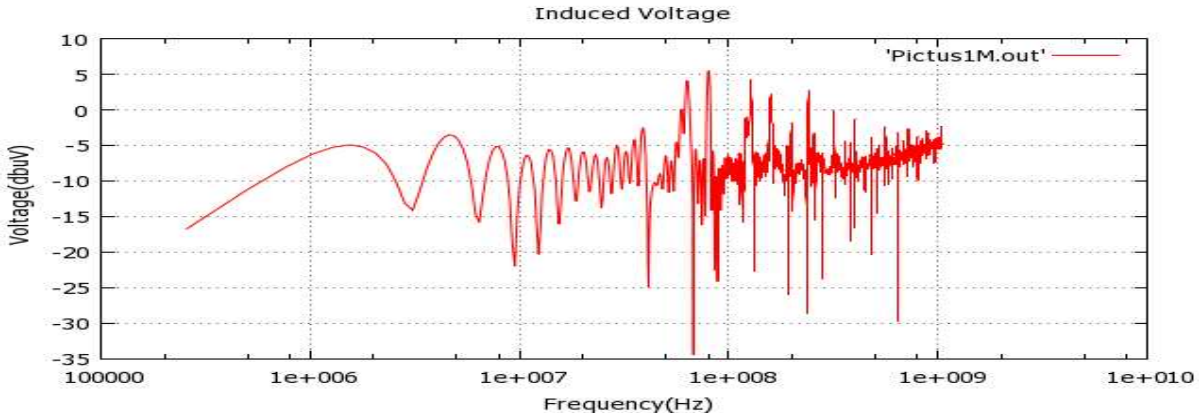

(b) Induced voltage computed by including the self-inductance caused due to internal field.

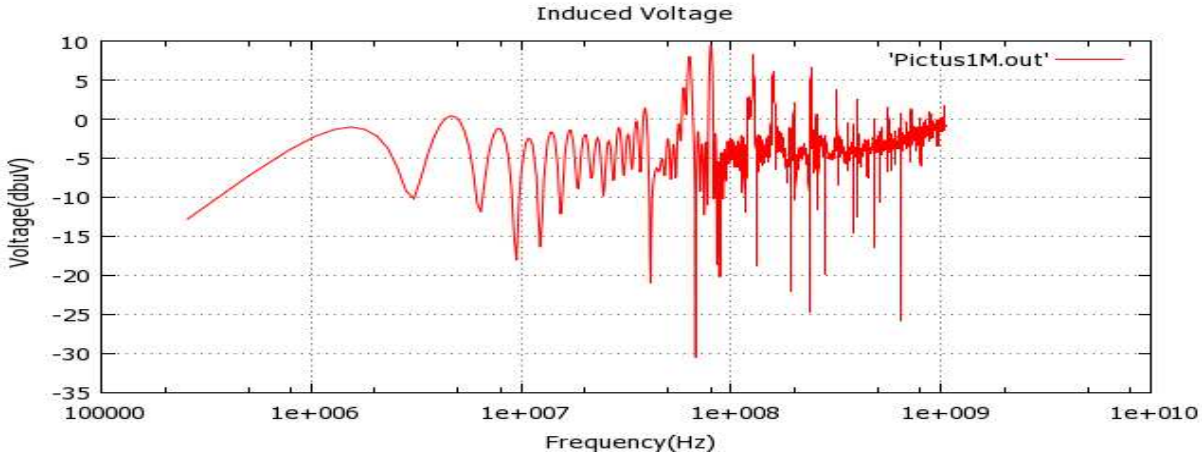

(c) Induced voltage of two loops separated with distance 0.5mm

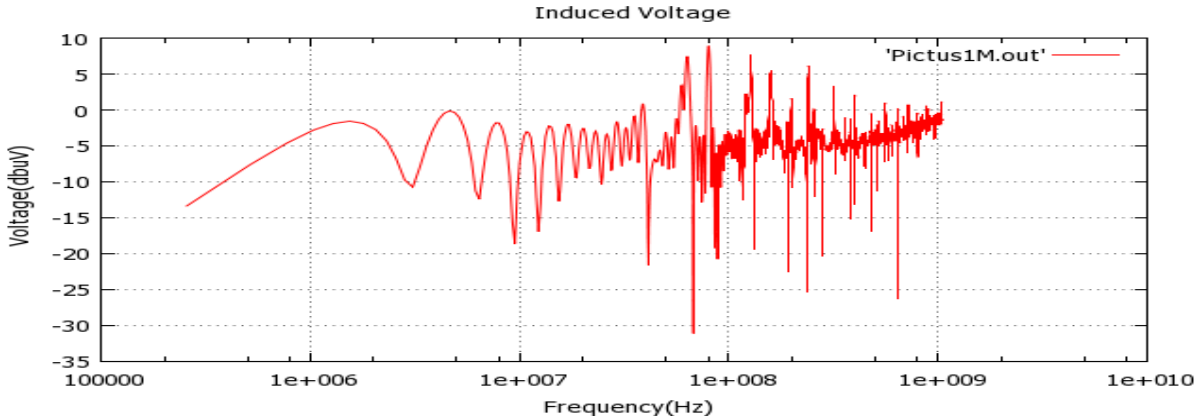

(d) Induced voltage of two loops separated with distance 0.3mm

Figure 5.6: Induced Voltage computed by modelling DUT using analytical expression.

In silicon results the maximum induced voltage is 12DBμV but using these tool we got 10DBμV .

It is very evident that the peak current plays a vital role in the radiated emission. Clock gating is one of the known techniques to reduce the peak current demand of the IC.

Some EMI reduction techniques are proposed in [25], Based on the simulation results we laid down the following design guideline for reducing the radiated emission of the IC.

1) Reduce the Peak current
    a. Clock Gating
    b. Skew
2) Lower value of the pulsed current from the package pins
    a. On-Chip Decoupling capacitor
3) Closest possible placement of the power supply pair

6. GTEM CELL

6.1 GTEM Cell*:*

The development of the GTEM cell in 1987 made EMC measurements possible at frequencies from dc up to several GHz which was a large progress against the limited usable frequency range of the TEM cell[21]. The new idea behind the GTEM cell was to avoid the corners that are the main reason for the limitation of the frequency range of the TEM cell .Therefore the main volume of the GTEM cell is only one section of a flattered rectangular transmission line. That means the length of inner and outer conductor is equal and thus the travel time along each conductor is equal. This property is also important factor for pulse type measurements, as the dispersion of the pulse is minimized.

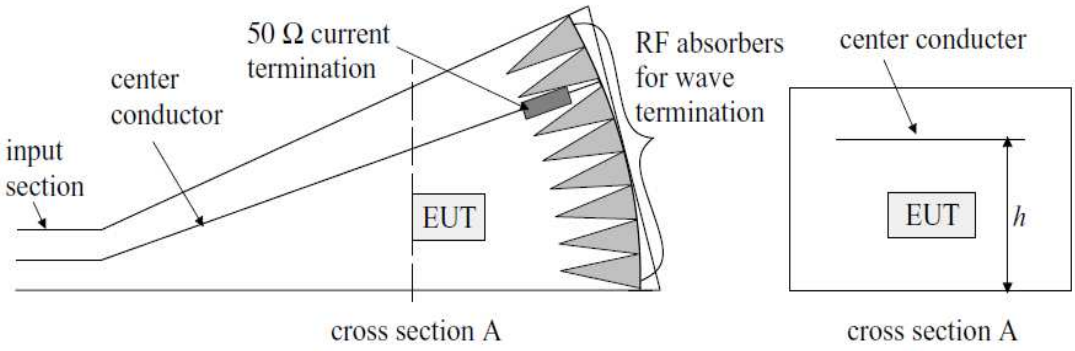

Figure 6.1: Schematic diagram of a GTEM cell .

Usually resonances arise in a closed cavity. Due to the flared shape this is not the case in a GTEM cell. The GTEM cell is like a former TEM cell well isolated and therefore neither contributes to nor is affected by any external interference. The cell typically has detachable input section, a so called apex. In the tip a standard 50Ω coaxial connector is mounted .In the input section then the transition from the standard 50Ω coaxial connector to the asymmetric rectangular waveguide with a flat center conductor is done.

The cell opens with an angle of 20^0 in the vertical plane and 30^0 in the horizontal plane respectively. Hence, the cross-sectional dimensions of the rectangular waveguide are a height to width ratio 2 to 3. The center conductor is vertically offset to increase the

usable test volume as opposed to a symmetric configuration .It is typically situated at three quarters of the cell height. The effect of this asymmetry an the field uniformity inside the volume below the center conductor is negligible against the advantage from the increased test volume.

For susceptibility testing an electronic device is placed in the testing volume and a CW to pulse generator is connected to the input of the cell according to the requirements. The propagation mode is TEM again but the waves are in the case slightly spherical. Due to the small opening angle they are very close to free space planar waves. Therefore the measurement procedure with a GTEM cell can be very well compared with the standard measurements like in anechoic rooms. The field uniformity inside the testing volume depends much on a low level reflections from the rare end of the cell. In order to absorb most of the energy that reaches the rear end a wideband matched termination is assembled at the rear wall.

For emission measurements the input of the GTEM cell is connected to the measuring equipment to monitor the output voltage as a result of emissions from the tested equipment inside the cell. It can be assumed that only the power directed towards the input along the longitudinal axis of the cell will be measured at the input. In any other direction than the input the waves arising from the DUT cannot propagate or are terminated by the hybrid termination in the rear end. In the reference environment for radiated emission measurements, which is typically free space or an OATS,. The actual electric and magnetic field strength in every direction is obtained through antennas at a certain direction. The results from a GTEM emission measurement consisting of output voltage data can be correlated with these environments.

Hence the GTEM cell can be used for susceptibility testing as well as for emission measurements for frequencies from dc up to several gigahertz due to broadband hybrid termination and the fact that there are no frequency limitations from mechanical dimensions as for the conventional TEM cell.

6.2 Characteristic Impedance*:*

The exact determination of the capacitance by the method of conformal transformation involves hyper geometric functions and four variable parameters; the process of obtaining numerical results would be so laborious that it has not been attempted. If the sides of the conductors are large compared with their spacing’s, the

distorted fields at the two ends along the same side of the inner conductor do not interact, and only one quarter of the cross section needs to be transformed. The inter-conductor capacitance can then be calculated as a combination of parallel-plate condensers formed by the walls of the conductors, plus excess capacitance caused by the disturbances of flux lines close to the corners. In fact, this method is valid whenever the short side of the inner conductor exceeds the spacing distances, as evidenced by the negligible amount of flux distortion at points not far away from the bend

When the sides of the conductors are large compared with the spacing's between them, one quarter of the cross section is to be considered. This portion of the cross-section then contributes a right-angled bend as shown in the figure 6.2. and forms the polygon in the z-plane bounded by the lines ABC and DEF, which are maintained at potential V and zero, respectively. It can be assumed that t=-∞ at a distant point on AB , t=-a at B, t=0 at a distant point on BC , and t=1 at E. The internal angles of the polygon are π/2 at B , zero at C and 3π/2 at E. The quantity a has to be determined from the geometry of the system . The Schwarz-Christoffel transformation which turns the boundary of the polygon into real axis in the t-plane shown in the figure 6.3 is

$$\frac{dz}{dt} = A_1(t-1)^{1/2}(t-0)^{-1}(t-a)^{-1/2} \qquad (6.1)$$

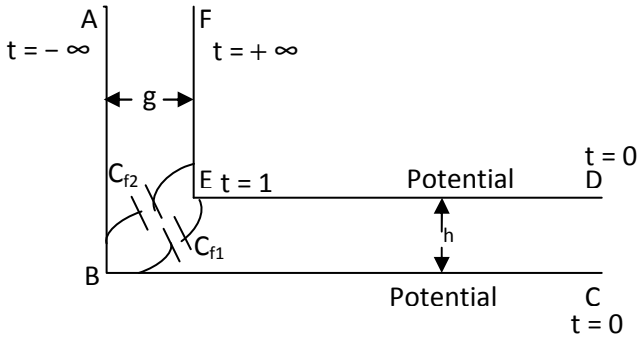

Figure 6.2: Z-plane

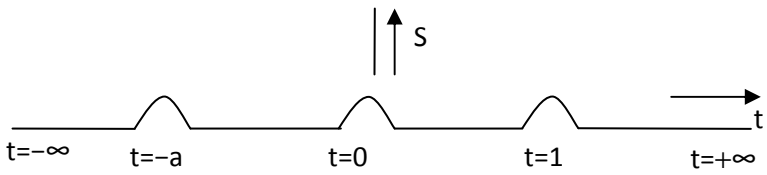

Figure 6.3: t-plane

The diagram in the w plane, shown in Fig.6.4 , consists of the real axis and a line parallel to it. The internal angle of the polygon is at t = 0, and is equal to zero. The transformation which turns this diagram into the real axis of the t plane is

$$\frac{dw}{dt} = B_1(t-1)^0(t-0)^{-1}(t-a)^0 \tag{6.2}$$

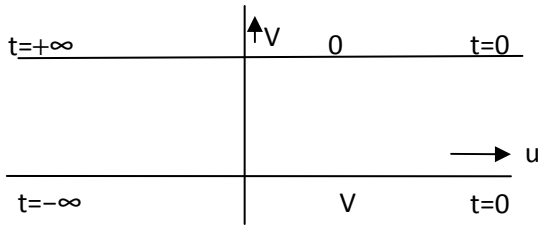

Figure 6.4: w-plane

which, upon integration and use of the boundary conditions, becomes

$$w = u + iv = \frac{V}{\pi} logt \tag{6.3}$$

To integrate let

$$X = (t-1)^{1/2}(t-a)^{-1/2} \tag{6.4}$$

And obtain

$$z = -2A_1\left(1/a\right)^{1/2} arc\ tan\left(a^{1/2}X\right) + A_1 log\frac{1+X}{1-X} \tag{6.5}$$

In which point E is chosen as the origin In the z plane Consideration of the values of t and X at point B leads to the relations

$$g = A_1\pi\,, h = A_1\pi\left(1/a\right)^{1/2}, \left(h/g\right)^2 = 1/a \tag{6.6}$$

Let P be a remote point on the line EF. The total charge on the strip EP per unit length in the direction normal to the plane of the paper is given by

$$Q_{EP} = \left(\frac{V}{\pi}\right)\epsilon\left[\log(a+1) + 2\left(1/a\right)^{1/2} arc\tan a^{1/2} - 2log2 + \frac{\overline{EP}}{A_1}\right] \tag{6.7}$$

If the flux lines were not disturbed, the charge on the strip EP would be, $\overline{EP}\epsilon\, V/g$ which the last term in the preceding expression is. The first three terms represent the excess charge caused by the flux disturbances. When the excess charge is divided by I_z and the relations in (38) are used, the fringing capacitance C_{f1} is obtained

$$C_{f1} = \frac{\epsilon}{\pi}\left[log\frac{g^2+h^2}{4h^2} + 2\left(\frac{h}{g}\right) arc\ tan\frac{g}{h}\right] \quad (6.8)$$

Similarly, the fringing capacitance associated with the horizontal side C_{f2} may be obtained from (39) by interchanging g and h.

$$C_{f2} = \frac{\epsilon}{\pi}\left[log\frac{g^2+h^2}{4g^2} + 2\left(\frac{g}{h}\right) arc\ tan\frac{h}{g}\right] \quad (6.9)$$

6.2.1 Line Capacitance

One corner of the line cross section assumes the shape of a right-angle bend; two successive transformations are necessary in this case as discussed in Appendix 1.3 d The first process transforms the z-plane polygon into the real axis of the t plane, and another transformation from the w plane to the t plane relates the potentials of the two conductors to values of t. The capacitance between the conductors is evaluated by letting z as well as it take critical values which depend on the particular problem.

In the L-shaped bend, the excess or fringing capacitance caused by the disturbance of flux lines emanating at the vertical side is expressed by

$$C_{f1} = \frac{\epsilon}{\pi}\left[log\frac{g^2+h^2}{4h^2} + 2\left(\frac{h}{g}\right) arc\ tan\frac{g}{h}\right] \text{ farads per meter} \quad (6.10)$$

where g is the lateral spacing and h the vertical spacing. Similarly, the equation for fringing capacitance produced by flux disturbance along half of the horizontal side is

$$C_{f2} = \frac{\epsilon}{\pi}\left[log\frac{g^2+h^2}{4g^2} + 2\left(\frac{g}{h}\right) arc\ tan\frac{h}{g}\right] \quad (6.11)$$

The capacitance between the vertical walls is

$$C_v = \epsilon\left(\frac{w}{h}\right) \quad (6.12)$$

$$C_h = \epsilon\left(\frac{b}{g}\right) \quad (6.13)$$

On the supposition that the conductor sides are large, the fringing capacitance depends only on the spacing's and not on the conductor dimensions. The total capacitance between the conductors is

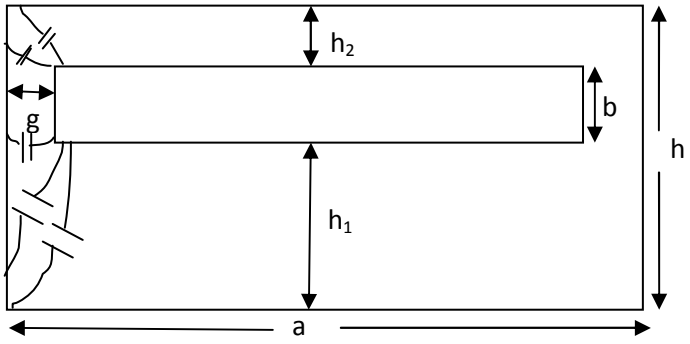

Figure 6.5: cross section of GTEM with finite thickness b indicating the capacitances in the half section

$$C = \epsilon\left(\frac{w}{h_1}+\frac{w}{h_2}+\frac{2b}{g}\right)+\frac{2\epsilon}{\pi}\left[\log\frac{g^2+{h_1}^2}{4{h_1}^2}+2\left(\frac{h_1}{g}\right)\arctan\frac{g}{h_1}\right]$$
$$+\frac{2\epsilon}{\pi}\left[\log\frac{g^2+{h_2}^2}{4{h_2}^2}+2\left(\frac{h_2}{g}\right)\arctan\frac{g}{h_2}\right]$$
$$+\frac{2\epsilon}{\pi}\left[\log\frac{g^2+{h_1}^2}{4g^2}+2\left(\frac{g}{h_1}\right)\arctan\frac{h_1}{g}\right]$$
$$+\frac{2\epsilon}{\pi}\left[\log\frac{g^2+{h_2}^2}{4g^2}\right.$$
$$\left.+2\left(\frac{g}{h_2}\right)\arctan\frac{h_2}{g}\right] \quad \text{farads per meter} \qquad (6.14)$$

6.2.2 **Inductance:**

The method of conformal transformation demonstrates that the fringing effect caused by charge concentration close to the edges of the inner conductor may be accounted for by the addition of correction lengths to the conductor sides. In Fig. 6.5, half of the vertical side of inner conductor should be increased by the amount

$$X_1 = \frac{1}{\pi}\left[g\log\frac{g^2+h^2}{4h^2}+2h\arctan\frac{g}{h}\right] = g\frac{C_{f1}}{\epsilon} \qquad (6.15)$$

The extension in half of the horizontal side, ,$X_2 = g\frac{C_{f2}}{\epsilon}$ can be obtained from (8) by interchanging g and h. When the effective lengths of the sides are used in the formula for calculating the inductance of parallel-plate transmission lines, the inductance of the rectangular line L is given by

$$L = \frac{L_v L_H}{L_v + L_H} \quad \text{henries per meter} \qquad (6.16)$$

In this expression, L_v and L_H are the inductances corresponding to the vertical and horizontal parallel-plate systems and are, respectively, given by

$$L_v = \frac{\mu g}{b+\frac{2}{\pi}\left[g\log\frac{g^2+{h_1}^2}{4{h_1}^2}+2\,arc\,tan\frac{g}{h_1}\right]} // \frac{\mu g}{b+\frac{2}{\pi}\left[g\log\frac{g^2+{h_2}^2}{4{h_2}^2}+2\,arc\,tan\frac{g}{h_2}\right]} \quad (6.17)$$

and

$$L_H = \frac{\mu h_1}{b+\frac{2}{\pi}\left[g\log\frac{g^2+{h_1}^2}{4g^2}+2g\,arc\,tan\frac{h_1}{g}\right]} // \frac{\mu h_2}{b+\frac{2}{\pi}\left[g\log\frac{g^2+{h_2}^2}{4g^2}+2g\,arc\,tan\frac{h_2}{g}\right]} \quad (6.18)$$

The capacitance and Inductance of the GTEM with negligible thickness can be computed by $C_0 = \lim_{b\to 0} C$

and $L_0 = \lim_{b\to 0} L$ (6.19)

After computing the Inductance and Capacitance we can compute characteristic impedance by

$$Z_0 = \sqrt{\frac{L_0}{C_0}} \quad (6.20)$$

or characteristic impedance can be computed from the capacitance , we know TEM wave propagates with a velocity of light , GTEM allows TEM (till higher order modes start propagation) by using the formula

$$Z_0 = \frac{1}{\upsilon C_0} \quad (6.21)$$

The characteristic impedance is computed and tested by computing for the TEM cell dimensions as shown in the figure 3.3 it is giving 49.6506. The dimensions used for computation of Fields are taken from [34] .

6.3 Electric Field and Magnetic Field Distribution in a GTEM cell*:*

The electric field distribution of GTEM cell is analysized using FEM in Maxwell 2D

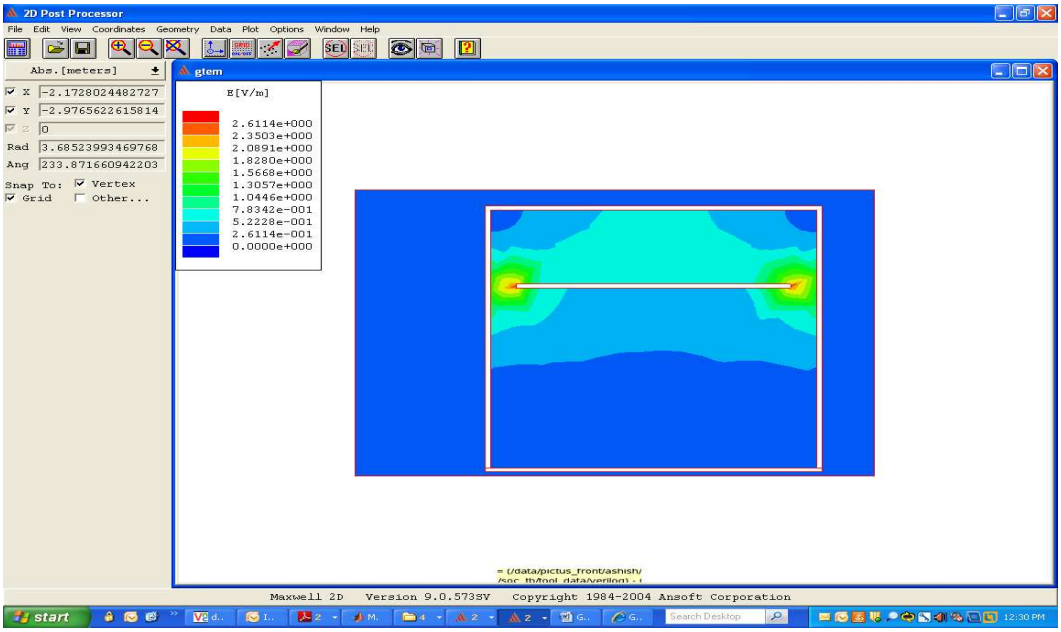

Figure 6.6:Electric Field distribution in a GTEM cell.

Flux Distribution :

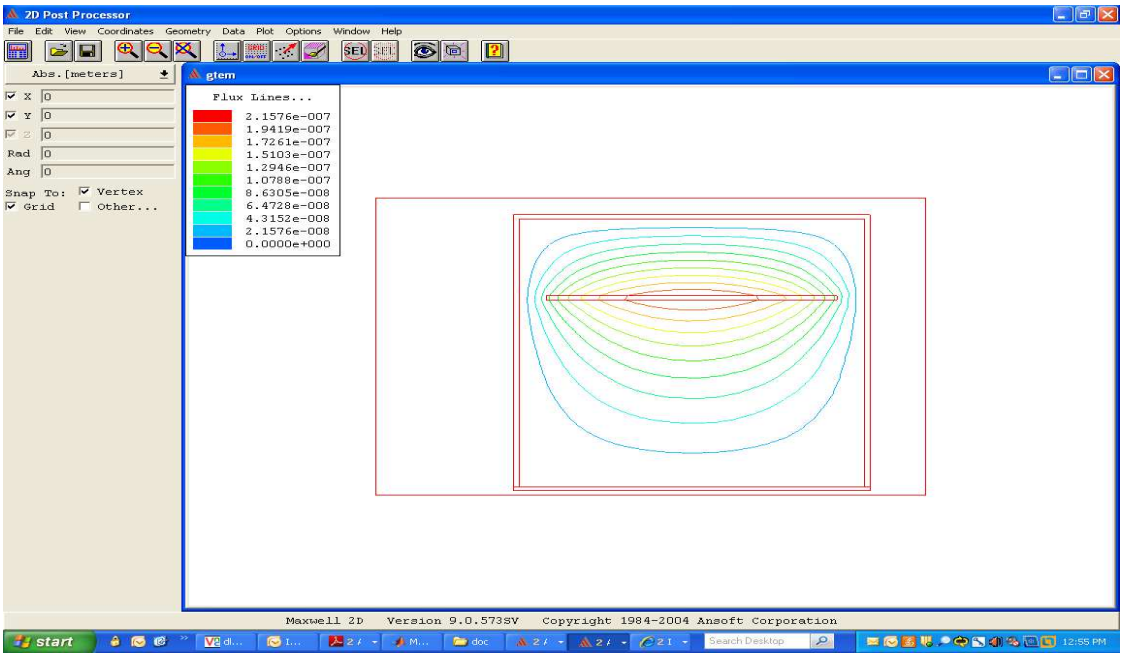

Figure 6.7:Flux lines in a GTEM cell

Magnetic Field Distribution:

The magnetic field distribution looks like

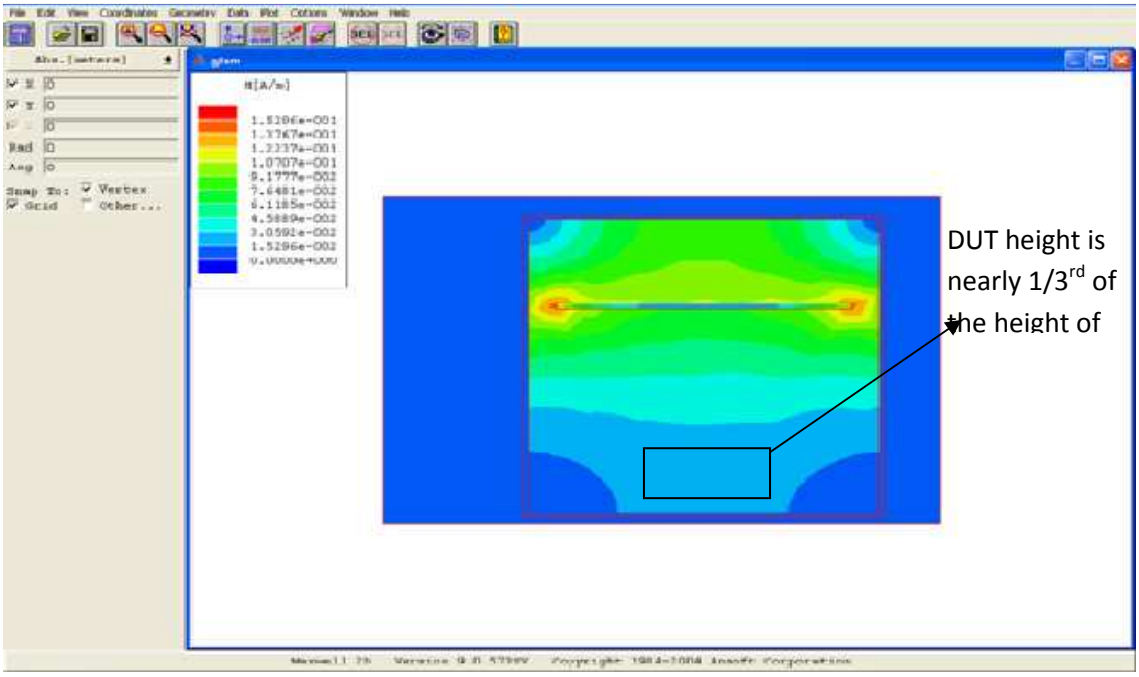

Figure 6.8: Magnetic Field in a GTEM cell.

From the above electric and magnetic field distributions, the placement of DUT in GTEM cell is at a height of one third from the bottom to the septum, because of uniformity of flux line and fields.

CONCLUSION:

In this project a new unified model has been shown which is suitable for the computer simulation. A rigorous and detailed analysis of the TEM cell and TEM mode of propagation is derived and based on these, parameters of the TEM cell is obtained. Based on the analysis of the excitation of the TEM mode of propagation the DUT is modelled as the excitation source of the TEM mode. An excellent correlation is found between the simulation results and silicon results.. Together with the coupled TEM cell and DUT model one can estimate the radiated emission of the IC at very early stage of the design . We further demonstrate how the various design parameter effects the radiated emission of the design. We laid down certain crucial design guideline which directly affects the radiated emission most. Since the model is very fast user can tune the various design parameter to obtain within the specs radiated emission. These new design specs can then be used further in the design cycle time to have a under the specification radiated emission of the IC. As already we have started the analysis on GTEM cell, the formulae for characteristic impedance has been done and some analysis on Fields are done by using FEM (Maxwell 2D).

FUTURE WORK:

We plan to take this work further and extending the results to GTEM cell which is new apparatus for measuring the radiated emission of the IC, and to model the same for different packages presently using for reducing EMI.

REFERENCES:

1. "Analysis and Computation of ELECTRIC AND MAGNETIC FIELD PROBLEMS", second edition by K.J.BINNS and P.J.LAWRENSON ,Pergamon press,1973.
2. J. C. Tippet et.al, Radiated Emission of Electrically Small Device in TEM Transmission Cell, IEEE Transaction on Electromagnetic Compatibility, Vol.EMC-18,No4, 1976
3. J. P. Muciolli, Investigation of the theoretical basis for using a 1GHz TEM cell to evaluate the emission of Integrated Circuits, IEEE Symp. For Electromagnetic Compatibility, CA, 1996
4. Andy Engel, Model of IC emission in TEM cell, IEEE Transaction on Electromagnetic Compatibility, Vol. EMC-34, No.1, 1995.
5. R. E. Collin, Foundation for Microwave Engineering. New York: IEEE Press, 1992.
6. Amit ROY et.al, Noise Coupling and Conducted Emission , ST TechWeek, 2010-12-13
7. Numerical Electromagnetics code(NEC) by G.J.Burke and A.J.Poggio of Lawarence Livemore Laboratory developed in the early 1970's by MBAssociates for the Naval Research Laboratory.
8. M.L. Crawford, *Generation of Standard EM Fields Using TEM Transmission Cells*, IEEE Trans. Electromagn. Compat., vol. EMC-16, pp. 189, Nov. 1974
9. R. F. Harrington, Field Computation by Moment Methods, Piscataway NJ:IEEE press,1993
10. R. E. Collin, Field Theory of Guided Waves. New York: IEEE Press, 1991.
11. "Excitation of a TEM Cell by a Vertical Electric Hertzian Dipole"by Perry F.Wilson ,David C.Chang and mark T.Ma at University of Colorado,NBS Technical Report 1037.
12. A thesis on "A TEM cell Design To Study Electromagnetic Radiation Exposure From Cellular Phones " by Nattaphong Boriraksantikul, Dr. Naz E. Islam, Thesis Advisor University of Missouri at in AUGUST 2008.
13. John David Jackson "Classical Electrodynamics " ,3rd edition John Wiley & Sons Publications ,1999.
14. "Electromagnetic Compatibility Procedure for Integrated Circuits- Integrated Circuit Radiated Emission Measurement Procedure," Society of Automotive Engineers (SAE), J1752/3, 1995
15. "Integrated Circuit Emission Measurement Procedure'" International Electro Technical Commission, Geneva, Switzerland, IEC 61967,2000.
16. "Limits and Methods of Measurement of the Radio Disturbance Characteristic of Information Technology Instrument," Bruxelles, Belgium, EN55022, 1995.
17. Franco Fiori et.al, Measurement of Integrated Circuit Conducted Emission by using a Transverse Conducted Cell (TEM)." IEEE Transaction on Electromagnetic Compatibility, Vol.43 , No.4, 2001
18. "The construction and application of a GTEM Cell" a thesis report by Clemens Icheln at Helsinki University of Technology in November,1995.
19. "Determination of Capacitance , Inductance and Characterstic Impedance of Rectangular Lines" by Tsung-shan Chen, IRE Transactions on Microwave Theory and Techniques,September,1960.
20. "Design And Characterization Of GTEM Cell" by Saswati Ghosh, Major R Singhley, S.V.K. Shastry', Ajay Chakrabarty at Proceedings of the International Conference on Electromagnetic Interference and Compatibility in 1999.

21. “Characterization Of A Gigahertz Transverse Electromagnetic Cell (GTEM Cell)” by D.C.Pande and P.K.Bhatt. at Proceedings of the International Conference on Electromagnetic Interference and Compatibility in 1997
22. A Dash of Maxwell’s by Glen Dash ,Ampyx LLC, Glen Dash at alum.mit.edu copyright 2000,2005 Amplyx LLC
23. “The Method of Moments : A Numerical Technique for Wire Antenna Design” by W.D.Rawle, Smiths Aerospace at High Frequency Electronics in 2006.
24. “Examinations of Higher Order Mode Cutoff Frequencies in Symmetrical TEM Cells” by Zhong Chen at IEEE in 2009.
25. “EMI Reduction Techniques” by Cameron Katrai and Chris Arcus in 1998 from Pericom Semiconductor Corporation ,Application Note-11.
26. “Input Impedance of a Probe Antenna in a TEM Cell” by Perry F.Wilson ,David C.Chang ,Mark T.MA, IEEE Transactions on Electromagnetic Compatibility, Vol. EMC-26, No. 4, November 1984.
27. “Field Measurements Made in an Enclosure” by Ernest E. Donaldson, William R. Free, Douglas W. Robertson, Jimmy A. Woody in Proceedings Of The IEEE, Vol. 66, No. 4, April 1978.
28. “Networks and Devices Using Planar Transmission Lines” by Franco Di Paolo ,Boca Raton: CRC Press LLC,2000.
29. “Theoretical and experimental investigations of Electromagnetic Field Distortion Due to a Perfectly Conducting Rectangular Cylinder in a Transverse Electromagnetic Cell” by motohisa kanda in Electromagnetic Fields Divison,NBS,1981.
30. “Characterization of Electrically Small Radiating Sources by Tests Inside a Trans-mission Line Cell” by Ippalapalli Sreenivasai, David C.Chang, Mark T .ma in NBS-Boulder, 1980.
31. F. Bowman, Introduction to Elliptic Functions with Applications. New York: Dover, 1961.
32. J. C. Tippet and D. C. Chang, "Radiation characteristics of dipole sources located inside a rectangular, coaxial transmission line," NBSIR 75-829, Jan. 1976.
33. J. Tippet and D. Chang, “Higher order modes in rectangular coaxial line with infinitely thin inner conductor,” National Bureau Standard Interagency Report, NBSIR 78-873, Boulder, CO, Mar. 1978.
34. “Analysis Of Gigahertz Tem Cell Using Finite-Difference Time-Domain (FDTD) Method”by Ondřej Franek, Vlastimil Navrátil, Zbyněk Raida , Dept. Of Radio Electronics, Brno University Of Technology.

APPENDIX-1

A cross-sectional view of a rectangular-coaxial-strip transmission line is shown in figure 3.4 with an x-y coordinate system superimposed.The strip of width 2w is located symmetrically inside a shielded enclosure of height 2b and width 2a and is assumed to have negligible thickness. In addition, the strip is located at a distance g from each vertical side wall and is embedded in a homogeneous dielectric of permittivity ε_0. The reason for choosing an asymmetrically located coordinate system is to facilitate obtaining approximate formulae for the capacitance. To determine the capacitance, the method of conformal transformation can be used, whereby the structure in figure 3.4 is transformed into a simpler configuration whose capacitance is already known. Since it is well known that the capacitance is invariant under a conformal transformation, the formulae obtained will also be applicable to the shielded stripline configuration of fig.3.4. Since we have symmetry with respect to the x axis ,we will calculate capacitance between the upper plate , A-F-E-D and the strip line ,B-C. the total capacitance is then twice this figure 3.4. Since we have effectively two capacitors in parallel. The region A-D-E-F may be mapped into the upper half of a complex t plane via the Schwartz-Christoffel transformation which due to symmetry can be used in terms of Jacobian elliptic functions The transformation is given by

$$mz = \int_0^t \frac{dt'}{[4t'(1-t')(1-k^2t')]^{1/2}} \qquad A1.1$$

Or alternatively given by

$$t = sn^2(mz, k) \qquad A1.2$$

Where sn is a Jacobian elliptic function of modulus k

$$m = \frac{K(k')}{b} \qquad A1.3$$

and

$$z = x + iy \qquad A1.4$$

here K(k) and $K(k')$ are complete elliptic integrals of the first kind of modulli k and k' ,respectively and

$$k' = [1 - k^2]^{1/2} \qquad A1.5$$

The modulus k can be determined from the requirement that

$$\frac{K(k)}{K(k')} = \frac{2a}{b} \qquad A1.6$$

Where the value of k^2 is tabulated for a given ratio $\frac{K(k)}{K(k')}$ .Under the transformation given by the region A-D-E-F in the z-plane is mapped into the upper half of the t-plane as shown in the figure A1.1.

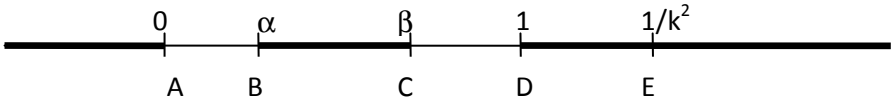

Figure A1.1: t-plane

Using (A1.2) and elliptic functions identities , α and β can be calculated as

$$\alpha = sn^2 mg = sn^2 \xi \qquad A1.7$$

And $$\beta = sn^2 m(2a - g) = \frac{cn^2 \xi}{dn^2 \xi} \qquad A1.8$$

Where

$$\xi = mg \qquad A1.9$$

And cn and dn are also jacobian elliptic functions each of which has modulus k .From convience we now make an intermediate transformation from the t-plane to a complex u plane defined by

$$u = \frac{\beta}{t}\left(\frac{t - \alpha}{\beta - \alpha}\right) \qquad A1.10$$

The u-plane is shown in fig A1.3 can be found using 10 and substituting t=1 .Thus

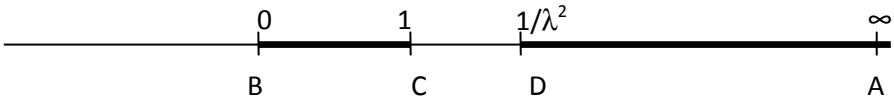

FigureA1.2:u-plane

$$\frac{1}{\lambda^2} = \beta\left(\frac{1-\alpha}{\beta-\alpha}\right) \qquad A1.11$$

And substituting for α and β from (A1.7) and (A1.8),we obtain

$$\lambda^2 = \frac{cn^2\xi - sn^2\xi dn^2\xi}{cn^2\xi(1-sn^2\xi)} \qquad A1.12$$

Using elliptic functions identities (A1.12) can be reduces to

$$\lambda^2 = 1 - k'^2\left(\frac{sn\xi}{cn\xi}\right)^4 \qquad A1.13$$

And defining a complementary modulus , λ' as

$$\lambda' = [1-\lambda^2]^{1/2} \qquad A1.14$$

We have from equ. (A1.13) and equ(A1.14)

$$\lambda' = k'\left(\frac{sn\xi}{cn\xi}\right)^2 \qquad A1.15$$

In the final transformation, we map the upper half of the u-pale into a rectangular region in a complex χ plane .The transformation is given by

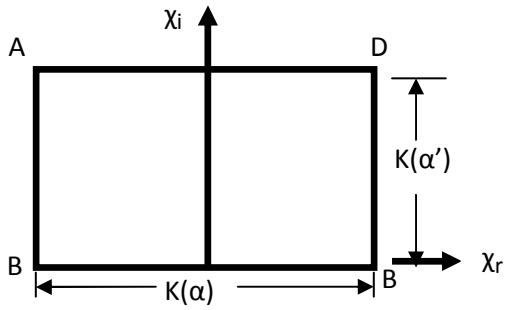

Figure A1.3: χ- plane

$$u = sn^2(\chi, \lambda) \qquad A1.16$$

And the χ plane is shown in figure A1.4 .from figure A1.4, it I evident that the capacitance is just given by the ordinary parallel-plate capacitor formulae . That is

$$\frac{C}{\varepsilon_0 L}\frac{K(\lambda)}{K(\lambda')} \qquad A1.17$$

Therefore, the total capacitance C_0 of the rectangular –coaxial-strip transmission line per unit length L is just that given by equ.(A1.17)

$$\frac{C}{\varepsilon_0 L} = 2\frac{K(\lambda)}{K(\lambda')} \qquad A1.18$$

Since equ(A1.6) and equ(A1.18) both involve ratios of complete elliptic integrals ,the following approximation is particularly useful

$$\frac{K(\delta)}{K(\delta')} \simeq \frac{1}{\pi}\ln\left(2\frac{1+\sqrt{\delta}}{1-\sqrt{\delta}}\right), \qquad \left(\delta^2 > \frac{1}{2}\right) \qquad A1.19$$

Using(A1.19) we can write expressions for (A1.6) and (A1.18) respectively as follows:

$$\frac{2a}{b} \simeq \frac{1}{\pi}\ln\left(2\frac{1+\sqrt{k}}{1-\sqrt{k}}\right), \qquad \left(k^2 > \frac{1}{2}\right) \qquad A1.20$$

$$\frac{C}{\varepsilon_0 L} = \frac{2}{\pi}\ln\left(2\frac{1+\sqrt{\lambda}}{1-\sqrt{\lambda}}\right), \qquad \left(\lambda^2 > \frac{1}{2}\right) \qquad A1.21$$

Equations (A1.20) and (A1.21) may be written alternatively as

$$\frac{4a}{b} = \frac{2}{\pi}\ln\left[2\left(1+\sqrt{k}\right)^2(1+k)\right] - \frac{2}{\pi}\ln(1-k^2) \qquad A1.22$$

$$\frac{C_0}{\varepsilon_0 L} \simeq \frac{2}{\pi}\ln\left[2\left(1+\sqrt{\lambda}\right)^2(1+\lambda)\right] - \frac{2}{\pi}\ln(1-\lambda^2) \qquad A1.23$$

subtracting (A1.22) from (A1.23) we obtain

$$\frac{C_0}{\varepsilon_0 L} - \frac{4a}{b} \simeq \frac{2}{\pi}\ln\left(\frac{k'^2}{\lambda'^2}\right) + \frac{2}{\pi}\ln\left\{\left(\frac{1+\sqrt{\lambda}}{1+\sqrt{k}}\right)^2\left(\frac{1+\lambda}{1+k}\right)\right\} \qquad A1.24$$

and substituting form (A1.15)

$$\frac{C_0}{\varepsilon_0 L} \simeq 4\left\{\frac{a}{b} + \frac{2}{\pi}\ln\left(\frac{cn\xi}{sn\xi}\right)\right\} + \frac{2}{\pi}\ln\left\{\left(\frac{1+\sqrt{\lambda}}{1+\sqrt{k}}\right)^2\left(\frac{1+\lambda}{1+k}\right)\right\} \qquad A1.25$$

in (A1.20) the restriction that $k^2 > 1/2$ is equivalent to requiring $(b/2a) < 1$, since when $k^2 = 1/2$, $K(k') = K(k)$.If we make the somewhat more stringent requirement that $(b/a) < 1$, which is equivalent to $k^2 > 0.97$, then (A1.25) may be further simplified by noting that fro $k \approx 1$

$cn\xi \simeq sech\xi$,$sn\xi \simeq tanh\xi$ and $\xi \simeq (\pi g/2b)$ thus

$$\frac{C_0}{\varepsilon_0 L} \simeq 4\left\{\frac{a}{b} - \frac{2}{\pi}\ln\left(sinh\frac{\pi g}{2b}\right)\right\} - \frac{\Delta C}{\varepsilon_0 L} \qquad A1.26$$

where

$$\frac{\Delta C}{\varepsilon_0 L} = \frac{2}{\pi} \ln\left\{\left(\frac{1+\sqrt{k}}{1+\sqrt{\lambda}}\right)^2 \left(\frac{1+k}{1+\lambda}\right)\right\} \qquad A1.27$$

An alternative form of (A1.26) may be obtained by using the following identity

$$sinh\left(\frac{\pi g}{2b}\right) = \frac{e^{(\pi g/2b)}}{\left[1 + coth\left(\frac{\pi g}{2b}\right)\right]}$$

With the result

$$\frac{C_0}{\varepsilon_0 L} \simeq 4\left\{\frac{w}{b} + \frac{2}{\pi} \ln\left(1 + coth\frac{\pi g}{2b}\right)\right\} - \frac{\Delta C}{\varepsilon_0 L} \qquad A1.28$$

In this form it is easy to identify the first term in (A1.29) as the plate capacitance between the stripline and the horizontal walls, and the second term as the fringing capacitance between the edges of the stripline and the side walls. For large gaps , the fringing approaches $(8/\pi) \ln 2$.

APPENDIX-2

The Numerical Electromagnetics Code (NEC-2) is a user-oriented computer code for analysis of the electromagnetic response of antennas and other metal structures. It is built around the numerical solution of integral equations for the currents induced on the structure by sources or incident fields. The code combines an integral equation for smooth surfaces with one specialized for wires to provide for convenient and accurate modeling of a wide range of structures.

A wire segment is defined by the coordinates of its two end points and its radius. Modeling a wire structure with segments involves both geometrical and electrical factors. Geometrically, the segments should follow the paths of conductors as closely as possible, using a piece-wise linear fit on curves.

Example loop construction :

4Nec2 is written using Fortran it executes in the form of cards ,

the below example is based on Fig 4.10.

```
CM
CE
GW  1   10   0      0   0       0      0   10.e-4  1.e-4
GW  2   5    0      0   10.e-4  5.e-4  0   10e-4   1.e-4
GW  3   10   5.e-4   0   10e-4   5.e-4  0   0       1.e-4
GE  1
GN  1
```

```
EK
EX    6     2     3     0     1     0     0
FR    0     0     0     0     1000  0
RP    0     10    4     1001  0.    0.    10.   30.
XQ
EN
```

CM card is used as a comment card and CE is for comment end.i.e. both CM and CE are used for comment lines

GW is used to construct geometry wire with '1' represents the tag number, '10' represents the number of segments , three consecutive fields "0 0 0" represents the first coordinate of the wire, followed by "0 0 10e-4" represents the second end of the wire.

1e-4 represents the radius of the wire.

GE indicates the end of construction of geometry

GN is used to represent the existance of ground plane

EX for exictation in which '6' represents the which identifies the position of the segment in a set of equal tag numbers, uniquely defines the source segment following '2' reprsents the tag number in which '3' the segment in that tag ,'0' represents the option number ,then '1' represents the real value and followed '0' represents the imaginary value.

FR reprsents the frequency i.e 1000MHz in this example

RP reprsents the Radiation pattern

XQ for intimating the execute command

EN for end of run

For more information refer to the reference manual of 4nec2 tool